A WARM JUPITER-SIZED PLANET TRANSITING THE PRE-MAIN SEQUENCE STAR V1298 TAU

Trevor J. David,[1] Ann Marie Cody,[2] Christina L. Hedges,[3] Eric E. Mamajek,[1,4] Lynne A. Hillenbrand,[5] David R. Ciardi,[6] Charles A. Beichman,[1,6] Erik A. Petigura,[5,*] Benjamin J. Fulton,[6] Howard T. Isaacson,[7] Andrew W. Howard,[5] Jonathan Gagné,[8,†] Nicholas K. Saunders,[9] Luisa M. Rebull,[10] John R. Stauffer,[11] Gautam Vasisht,[1] and Sasha Hinkley[12]

[1]Jet Propulsion Laboratory, California Institute of Technology, 4800 Oak Grove Drive, Pasadena, CA 91109, USA
[2]NASA Ames Research Center, Moffett Field, CA 94035, USA
[3]Bay Area Environmental Research Institute, P.O. Box 25, Moffett Field, CA 94035, USA
[4]Department of Physics & Astronomy, University of Rochester, Rochester, NY 14627, USA
[5]Department of Astronomy, California Institute of Technology, Pasadena, CA 91125, USA
[6]Caltech/IPAC-NASA Exoplanet Science Institute, Pasadena, CA 91125, USA
[7]Astronomy Department, University of California, Berkeley, CA 94720, USA
[8]Institut de Recherche sur les Exoplanètes, Département de Physique, Université de Montréal, Montréal QC, H3C 3J7, Canada
[9]NASA Ames Research Center, Moffet Field, CA 94035, USA
[10]Caltech/IPAC-IRSA, Pasadena, CA 91125, USA
[11]Caltech/IPAC-SSC, Pasadena, CA 91125, USA
[12]University of Exeter, Physics Department, Stocker Road, Exeter EX4 4QL, UK

ABSTRACT

We report the detection of V1298 Tau b, a warm Jupiter-sized planet ($R_P = 0.90 \pm 0.05\ R_{\rm Jup}, P = 24.1$ days) transiting a young solar analog with an estimated age of 23 million years. While hot Jupiters have been previously reported around young stars, those planets are non-transiting and near-term atmospheric characterization is not feasible. The V1298 Tau system is a compelling target for follow-up study through transmission spectroscopy and Doppler tomography owing to the transit depth (0.5%), host star brightness ($K_s = 8.1$ mag), and rapid stellar rotation ($v \sin i = 23$ km s^{-1}). Although the planet is Jupiter-sized, its mass is presently unknown due to high-amplitude radial velocity jitter. Nevertheless, V1298 Tau b may help constrain formation scenarios for at least one class of warm Jupiters, providing a window into the nascent evolution of giant planet interiors and atmospheres.

1. INTRODUCTION

The properties and demographics of young exoplanets may potentially reveal valuable insights into the physics of planet formation. For giant planets, in particular, the post-formation radii, temperatures, and luminosities may help to constrain how planets accrete

Corresponding author: Trevor J. David
trevor.j.david@jpl.nasa.gov

* NASA Hubble Fellow
† Banting Fellow

gaseous envelopes and perhaps whether or not they possess rocky cores (e.g. Burrows et al. 1997; Baraffe et al. 2003; Marley et al. 2007; Fortney et al. 2007; Fortney & Nettelmann 2010; Spiegel & Burrows 2012; Mordasini 2013; Mordasini et al. 2017). For planets of smaller sizes ($\lesssim 4\ R_\oplus$), a valley in the distribution of planetary radii (Fulton et al. 2017) has fueled speculation about the relative importance of photo-evaporation (Owen & Wu 2013; Lopez & Fortney 2013), planetary impacts (Schlichting et al. 2015), and core-envelope interactions (Ginzburg et al. 2018; Gupta & Schlichting 2018) to the evolution of exoplanetary atmospheres.

Discerning which of the proposed processes are important to the evolution of exoplanets, and which are not, requires studying planetary systems of a variety of ages. For this reason, the task of identifying exoplanets in stellar associations with well-defined ages has attracted significant attention lately (Ciardi et al. 2018; Curtis et al. 2018; Libralato et al. 2016; Livingston et al. 2018, 2019; Mann et al. 2016a, 2017, 2018; Obermeier et al. 2016; Pepper et al. 2017; Quinn et al. 2012, 2014; Rizzuto et al. 2018; Vanderburg et al. 2018).

At the youngest ages (<100 Myr), when observed exoplanet properties might place the strongest constraints on formation theories, there are only a small number of known exoplanets; several young giant planets have been discovered via direct imaging (see Bowler 2016, for a review) while there are only five validated or candidate close-in exoplanets with securely measured ages. Three of the close-in planets are hot Jupiters detected through radial velocity monitoring of T Tauri stars (Donati et al. 2016; Johns-Krull et al. 2016; Yu et al. 2017), one is a candidate transiting hot Jupiter of controversial nature (van Eyken et al. 2012; Yu et al. 2015), and the other is a Neptune-sized planet transiting a pre-main sequence star (David et al. 2016; Mann et al. 2016b).

NASA's *Kepler Space Telescope* observed thousands of young stars during its extended *K2* mission (Howell et al. 2014). For most of these stars, *K2* provided time series photometry with unprecedented precision, cadence, and duration. Using astrometry from the second data release of the *Gaia* mission (Gaia Collaboration et al. 2018) and a Bayesian membership algorithm (Gagné et al. 2018), we searched the entire *K2* source catalog for high-probability members of young moving groups and stellar associations. Our search yielded 432 candidate members of the Taurus-Auriga star-forming region, including V1298 Tau. In an automated search for periodic transits or eclipses within the the *K2* photometry for these candidate members we detected 0.5% dimming events which last 6.4 hours and repeat every 24.1 days within the light curve of V1298 Tau (Figure 1). Follow-on observations confirm the periodic transits are most probably due to a Jovian-sized planet orbiting at a separation of 0.17 AU from V1298 Tau.

In §2 we describe the *K2* time series photometry from which the planet V1298 Tau b was detected and the follow-on observations used to validate the planet. Our analysis of these observations and assessment of false-positive scenarios is described in §3. We place the planet V1298 Tau b in context in §4, and present our conclusions in §5.

## 2. OBSERVATIONS AND CHARACTERIZATION OF THE DATA

2.1. *K2 time series photometry*

The *Kepler* space telescope observed V1298 Tau during Campaign 4 of the *K2* mission (Howell et al. 2014), between 2015 February 7 and 2015 April 23 UTC. The star was included in the following Guest Observer programs: GO4020 (Stello), GO4057 (Prša), GO4060 (Coughlin), GO4090 (Caldwell), GO4092 (Brown), and GO4104 (Dragomir). Telescope pointing drift combined with intra-pixel detector sensitivity variations imprint systematic artifacts upon *K2* time series photometry. We corrected for these systematic effects using the everest 2.0 pipeline (Luger et al. 2018), which employs a variant of the pixel-level decorrelation (PLD) method (Deming et al. 2013). We also confirmed the transits are present in the raw uncorrected photometry using the interactive lightkurve tool (Barentsen et al. 2019), as well as in independent reductions of the data using the k2sc (Aigrain et al. 2016) and k2phot (Petigura et al. 2018) pipelines.

The *K2* time series photometry is characterized by quasi-periodic variations with a peak-to-trough amplitude of $\sim$6% and a period of 2.851 ± 0.050 days (§3.3), values typical of similarly young stars (Rebull et al. 2018). We attribute this variability to stellar rotation and a non-axisymmetric distribution of spots on the stellar surface. The photometry also reveal several flares over the 70.8 day observing baseline, confirming that the star is magnetically active. Prior to fitting transit models to the photometry, we removed the intrinsic stellar variability through Gaussian process (GP) regression. For the GP we used a Matérn-3/2 kernel with an additional white noise term, using a white noise amplitude of 243 ppm, red noise amplitude of 1.215×10^5 counts, and red noise timescale of 29.17 days. The transits were masked prior to both the PLD detrending and the final GP regression to prevent under- or over-fitting the transit signal.

From inspection of systematics-corrected light curves using both the everest 2.0 and k2sc pipelines we find that there are several outlying or missing in-transit measurements (Figure 2). Most notably, observations of the third transit ingress (cadences 106358 through 106361), are missing due to the fact that the *Kepler* spacecraft was not in fine-pointing mode and did not acquire data.[1]

---

[1] Quality flag meanings are summarized in Table 2.3 of the *Kepler* archive manual (https://archive.stsci.edu/kepler/manuals/archive_manual.pdf) and may be interpreted with software available at https://gist.github.com/barentsen/9b5a7b51f48e026e3af5
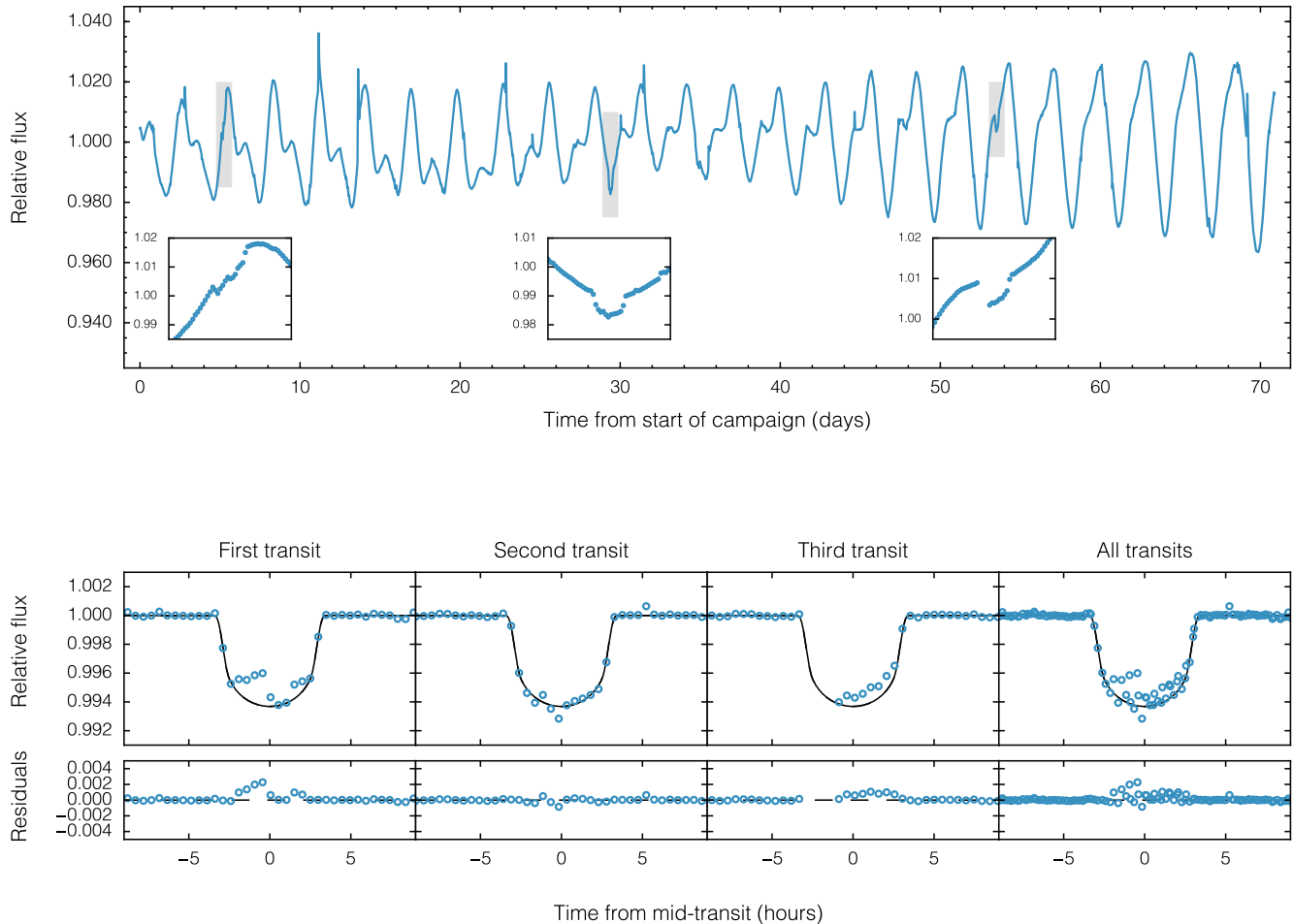
Figure 1. K2 time series photometry of V1298 Tau. *Top:* Systematics-corrected *K2* photometry of V1298 Tau from the EVEREST 2.0 pipeline. Inset panels show day-long windows around individual transits, also indicated by the grey shaded regions. *Bottom:* Folded and individual transits of V1298 Tau b (points) with a transit model fit (solid line) found from excluding anomalous observations. Residuals of this fit are shown below each panel. Observations missing from the ingress of the third transit are due to an interruption in data acquisition which affected all targets in Campaign 4.

The outlying observations during the first transit, which are present in both the EVEREST 2.0 and K2SC light curves, are not as easily explained. Transit profile distortions may be systematic or astrophysical in nature, and possibly the result of both effects. Quality flags from the *K2* photometry indicate that some observations taken during the first transit were affected by cosmic rays or thruster firings. However, observations closely spaced in time which also appear to be outliers were not affected by such systematics and thruster firings in particular are naturally detrended with the pixel-level decorrelation approach of the EVEREST 2.0 pipeline. It is possible that the outliers are instead astrophysical in nature, arising from the planet occulting active regions on the stellar surface. The transit depth is reduced when the planet crosses a dark starspot and increased if the planet crosses a bright plage or flaring

region. With only three transits, we can not conclusively attribute any outliers to spot-crossing events, but the light curve of V1298 Tau is indeed suggestive of a non-axisymmetric spotted stellar surface.

2.2. *High-resolution imaging*

We observed V1298 Tau with infrared high-resolution adaptive optics (AO) imaging at Keck Observatory. The Keck Observatory observations were made with the NIRC2 instrument on Keck-II behind the natural guide star AO system. The observations were made on 2018 Nov 22 UT in the standard 3-point dither pattern that is used with NIRC2 to avoid the left lower quadrant of the detector which is typically noisier than the other three quadrants. The dither pattern step size was $3''$ and was repeated twice, with each dither offset from the previous dither by $0.5''$.
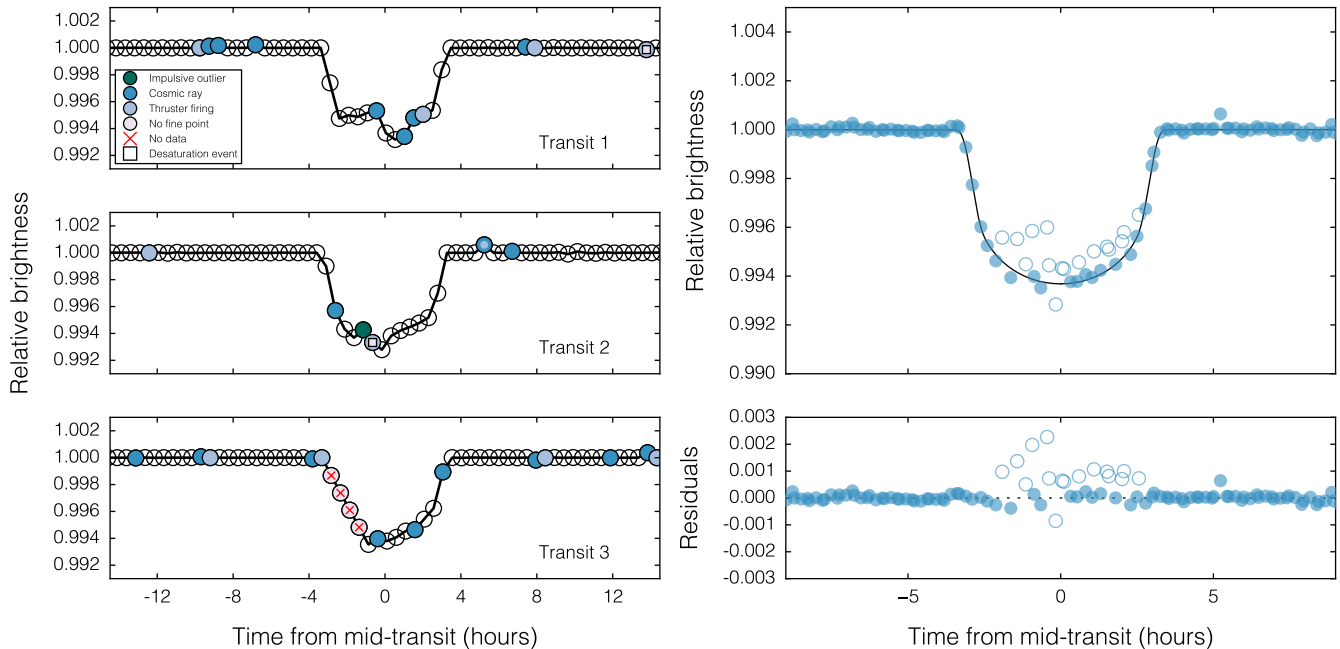
Figure 2. *Left:* Individual transits of V1298 Tau observed with *K2*. The light curve shown is one possible realization from the EVEREST 2.0 pipeline. Measurements affected by various telescope systematics are as indicated by the figure legend. *Right:* Transit fit (black line) with observations included in the final fit shown as filled circles, and excluded observations as open circles.

The observations were made in the narrow-band Br-γ filter ($\lambda_o = 2.1686; \Delta\lambda = 0.0326\mu m$) with an integration time of 1.25 seconds with one coadd per frame for a total of 11.25 seconds on target and in J-cont ($\lambda_o = 1.2132; \Delta\lambda = 0.0198\mu m$) with an integration time of 5 seconds with one coadd per frame for a total of 45 seconds on target. The camera was in the narrow-angle mode with a full field of view of $\sim 10''$ and a pixel scale of approximately 9.9442 mas per pixel. The Keck AO observations show no additional stellar companions were detected to within a resolution $\sim 0.05''$ full width at half maximum (FWHM).

The sensitivities of the final combined AO image were determined by injecting simulated sources azimuthally around the primary target every $45°$ at separations of integer multiples of the central source's FWHM (Furlan et al. 2017). The brightness of each injected source was scaled until standard aperture photometry detected it with 5σ significance. The resulting brightness of the injected sources relative to the target set the contrast limits at that injection location. The final 5σ limit at each separation was determined from the average of all of the determined limits at that separation; the uncertainty on the 5σ limit was set by the root mean square dispersion of the azimuthal slices at a given radial distance.

2.3. *Spectroscopic observations and radial velocities.*

We observed V1298 Tau on 9 nights between 3 November 2018 and 26 January 2019 UTC using the High Resolution Spectrograph (HIRES) on the Keck-I telescope (Vogt et al. 1994). We first acquired a spectrum for characterization purposes on 3 November 2018, before commencing precision radial velocity (PRV) monitoring with the iodine cell. Our characterization spectrum has a resolution of $R \approx 36,000$ between ~ 4800–9200 Å. For the PRV observations, a template spectrum with resolution of $R \approx 80,000$ was obtained for use with the California Planet Survey RV pipeline (Howard et al. 2010). The PRV observations themselves have a resolution of $R \approx 50,000$ between ~ 3600–8000 Å. The PRVs for V1298 Tau are presented in Table 1. From those data we measured the optical radial velocity jitter to be $\sigma_{RV} = 216$, 71, and 5 m s^{-1} over 5.2 days, 10 hours, and 30 minutes, respectively. While a measurement of the planet mass is precluded by the large stellar variability, we derive an upper limit in §3.11.

For the first epoch of spectroscopic observations, the radial velocity was derived by cross-correlating the spectrum with a radial velocity standard (Table 2). For this measurement we used the G2 type standard HD 3765 (Nidever et al. 2002), which we observed with HIRES on the same night and in the same spectrograph configuration. Uncertainty was quantified from the dispersion among measurements relative to different standards,

and over 24 different spectral orders. The sky-projected rotational velocity was also estimated from this spectrum by artificially broadening the spectral standard Gl 651 (SpT = G8) using the standard Gray broadening profile (Gray 2005) with $\epsilon = 0.6$. Velocities between 9 and 50 km s^{-1} were sampled and the best-fit value for $v \sin i$ was determined by minimizing residuals, suggesting 23 ± 2 km s^{-1}.

3. ANALYSIS

3.1. Association membership and kinematics

V1298 Tau was first proposed as a young star and candidate Taurus-Auriga member based on a detection of its X-ray emission from the *ROSAT* All-Sky Survey (Wichmann et al. 1996). The star's relative youth (age $\lesssim$100 Myr) was then verified on the basis of strong lithium 6708 Å absorption (Wichmann et al. 2000). Taurus-Auriga, at ~3 Myr, contains both classical T Tauri stars in the process of forming planets as well as weak-line T Tauri stars lacking accretion signatures. V1298 Tau, an early K-type star which has no significant infrared excess and exhibits Hα in absorption, could fit into the latter category.

Alternatively, while V1298 Tau is young, it may be significantly older than 3 Myr. The existence of an older and more spatially distributed pre-main sequence population in the vicinity of Taurus has been recognized (e.g. Hartmann et al. 1991; Slesnick et al. 2006; Kraus et al. 2017; Zhang et al. 2018), but a recent kinematic analysis enabled by *Gaia* suggests the older population is physically unrelated to the Taurus-Auriga association (Luhman 2018). Many of the more spatially distributed candidate young stars likely belong to a newly identified, older association preliminarily named Group 29 (Luhman 2018), to which V1298 Tau was proposed to belong (Oh et al. 2017).

The *Gaia* astrometry and barycentric radial velocity of V1298 Tau were used to estimate the star's probability of membership to the Taurus-Auriga (Tau-Aur) star-forming region. Using the BANYAN Σ classification tool (Gagné et al. 2018), we found that V1298 Tau has a 99.8% probability of belonging to Taurus and a 0.2% probability of being a field star. However, BANYAN Σ utilizes an inclusive model for Taurus-Auriga and does not yet take into account the aforementioned analysis of kinematic substructure in the association.

From the Hertzsprung-Russell diagram position (Figure 3), stellar kinematics (Figure 4), and spatial location relative to the Taurus molecular clouds (Figure 4), we conclude that V1298 Tau is a member of Group 29, an older association in the foreground of Taurus-Auriga. The age of Group 29 is estimated to be less
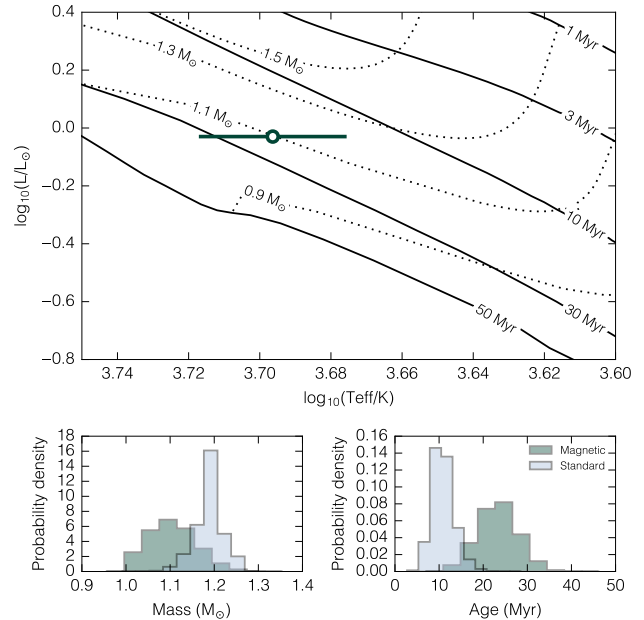
Figure 3. *Top:* V1298 Tau (blue point) in a theoretical H-R diagram. Isochrones (solid lines) and mass tracks (dotted lines) from Dartmouth models including the effects of magnetic fields (Feiden 2016) are shown. *Bottom:* Mass and age distributions from Monte Carlo simulations for V1298 Tau according to magnetic (green) and standard (blue, Dotter et al. 2008) Dartmouth evolutionary models. Given the precise parallax and near-infrared photometry, the uncertainties in mass and age are dominated by the error in $T_{\rm eff}$ and model systematics.

than 45 Myr by comparison with known moving groups in a color-absolute magnitude diagram (Luhman 2018, see also Figure 5). We note, however, that the precise age and substructure of this group has not been fully explored. A comparison of Li I 6708 Å equivalent widths among young stars compiled from the literature[2] supports an upper limit of 45 Myr for the age of V1298 Tau (Figure 6).

3.2. Stellar parameters

We determined the stellar effective temperature, luminosity, and radius from 2MASS near-infrared photometry, the trigonometric parallax, and empirical relations for pre-main sequence stars (Pecaut & Mamajek 2013). From a three-dimensional map of the local interstellar medium, we determined the color excess

---

[2] Li 6708 Å equivalent widths and temperatures/spectral types were compiled from Soderblom et al. (1993); Jones et al. (1996); Barrado y Navascués et al. (2001); Randich et al. (2001); Mentuch et al. (2008); Yee & Jensen (2010); Malo et al. (2013); Jeffries et al. (2013); Binks & Jeffries (2014); Kraus et al. (2014, 2017); Bouvier et al. (2018).

Table 1. Keck/HIRES precision radial velocities of V1298 Tau

Observation	UTC Date	JD	RV	σ_{RV}
			(m s^{-1})	(m s^{-1})
rj310.68	2018-11-16	2458438.94547	+459.27	6.23
rj311.73	2018-11-21	2458443.81966	-233.24	4.73
rj311.113	2018-11-21	2458443.95650	-67.81	3.91
rj311.114	2018-11-21	2458443.96733	-56.12	4.26
rj311.115	2018-11-21	2458443.97835	-64.60	4.00
rj311.172	2018-11-21	2458444.15574	-37.38	5.58
rj314.102	2018-12-24	2458476.80809	+147.66	8.48
rj315.63	2018-12-26	2458479.00517	+14.88	7.80
rj316.90	2019-01-07	2458490.79036	+191.34	8.39
rj316.376	2019-01-08	2458491.75402	-101.69	7.34
rj317.81	2019-01-25	2458508.91881	-136.91	8.72
rj317.398	2019-01-26	2458509.78912	+127.77	8.76
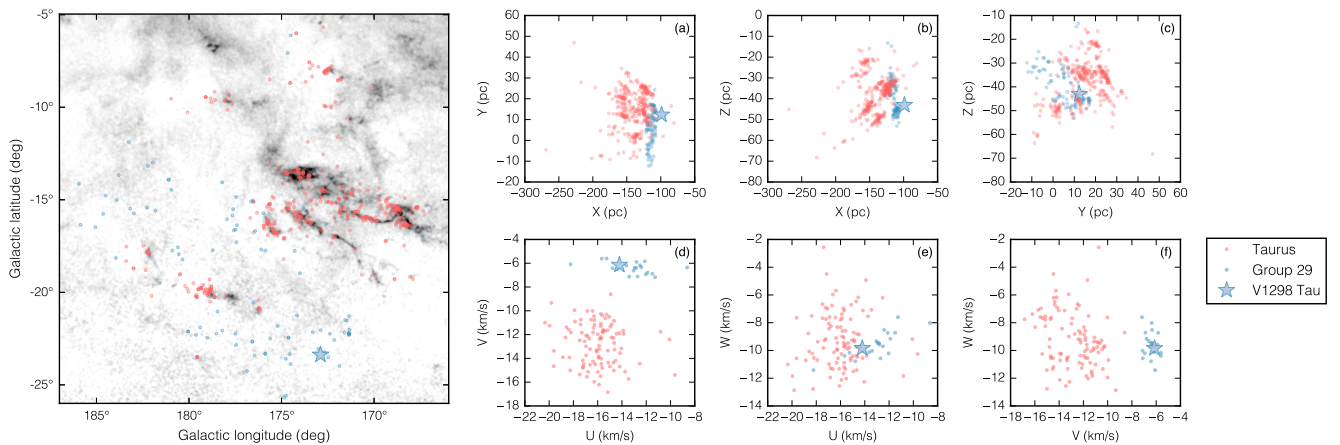
Figure 4. *Left:* Galactic coordinates of V1298 Tau (blue star) relative to Taurus-Auriga members (red circles) and proposed members of Group 29 (blue circles). Stellar positions are overlaid on an extinction map (Dobashi et al. 2005). *Right:* Galactic positions and kinematics of V1298 Tau, Taurus, and Group 29. *(a-c)* The galactic positions of Taurus members and Group 29 candidate members relative to V1298 Tau. The narrow range in X spanned by Group 29 candidates is a result of a stringent parallax cut, and there are likely more unidentified members in the foreground. *(d-f)* Galactic kinematics of Taurus members and Group 29 candidate members relative to V1298 Tau.

along the line-of-sight to V1298 Tau to be $E(B - V)$ = 0.024 ± 0.015 mag (Lallement et al. 2014; Capitanio et al. 2017). Assuming an extinction law (Yuan et al. 2013), we determined the J-band extinction to be A_J = 0.019 ± 0.010 mag and the star's intrinsic $J - K_s$ color $(J - K_s)_0$ = 0.582 ± 0.032 mag. From the intrinsic $(J - K_s)_0$ color and linear interpolation between empirical pre-main sequence relations, we determined the effective temperature and the appropriate J-band bolometric correction. Using the extinction-corrected J-band magnitude we then calculated the bolometric luminosity. From the luminosity and effective tempera-

ture, we determined the stellar radius from the Stefan-Boltzmann law. Our adopted temperature is consistent with previous determinations, which range from 4920–5080 K (Davies et al. 2014; Wichmann et al. 2000; Wahhaj et al. 2010; Palla & Stahler 2002). The spectral type has been reported as K1 (Wichmann et al. 1996) and K1.5 (Kraus et al. 2017), and we find the HIRES spectrum to be most consistent with K0. The mass, estimated below, suggests V1298 Tau will evolve to become a late F-type or early G-type main sequence star.

We used stellar evolution models to estimate the mass and age of V1298 Tau in a theoretical Hertzsprung-
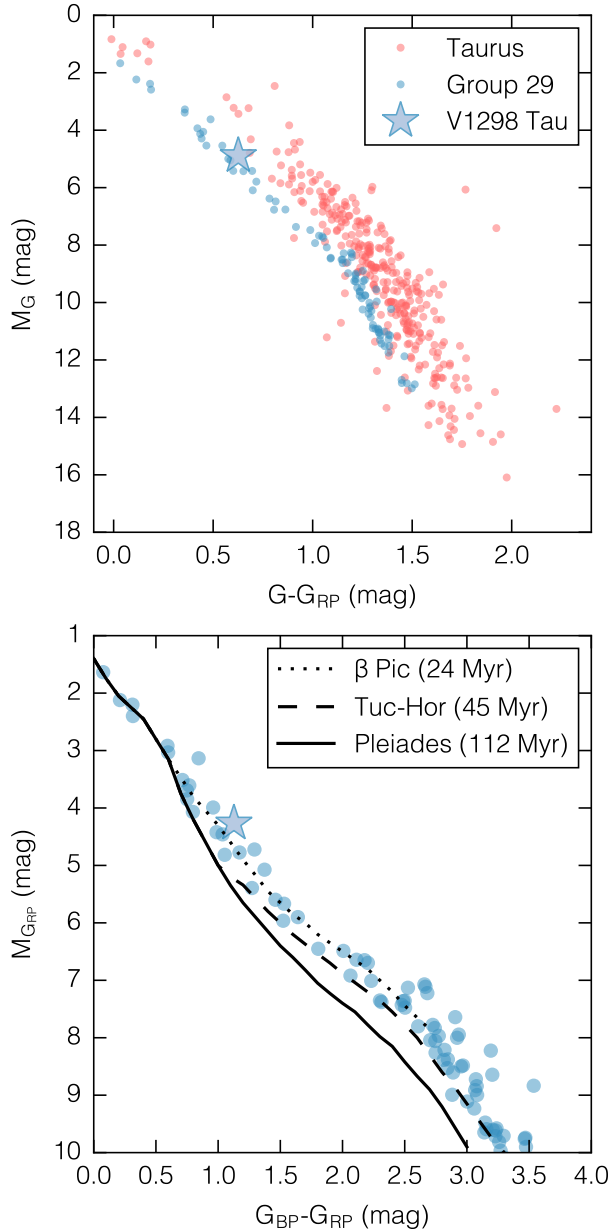
Figure 5. *Top:* V1298 Tau (blue star) compared to Taurus-Auriga members (red circles) and proposed members of Group 29 (blue circles) in a color-absolute magnitude diagram. *Bottom:* V1298 Tau in comparison to empirical fits to the single star sequences of two moving groups and one open cluster (Luhman 2018).

Russell diagram. The pre-main sequence phase of evolution is particularly uncertain in theoretical models due to a dearth of calibrators. One major uncertainty regards the importance of magnetic fields. To estimate the magnitude of the model uncertainty for V1298 Tau we present two determinations of mass and age using models that neglect and account for magnetic fields (Dot-

ter et al. 2008; Feiden 2016). Standard models predict a mass and age of $M_* = 1.19 \pm 0.03\ M_\odot$ and $\tau = 11 \pm 3$ Myr, respectively. By comparison, magnetic models predict a mass of $M_* = 1.10 \pm 0.05\ M_\odot$ and an age of $\tau = 23 \pm 4$ Myr, which we ultimately adopt (Figure 3). Uncertainties in all derived stellar parameters were calculated from Monte Carlo simulations modeling input parameters as normal distributions with widths corresponding to the errors in the photometry, parallax, and extinction. The derived stellar parameters are summarized in Table 2.

3.3. *Stellar rotation and activity*

We infer a stellar rotation period of $P_{\rm rot} = 2.851 \pm 0.050$ days from a Lomb-Scargle periodogram (Lomb 1976; Scargle 1982) of the *K2* time series photometry (Figure 7). The period and uncertainty were determined from the mean and the half-width at half-maximum of a Gaussian fit to the periodogram peak, respectively. An autocorrelation function (ACF) of the *K2* light curve suggests a rotation period of $P_{\rm rot} = 2.8605 \pm 0.0082$ days, consistent within 1σ. In this case the period is determined from the slope of a linear fit to the first four peaks of the ACF, with the uncertainty determined from the root mean square of the fit residuals. The period we report is in agreement with a previously published value (Grankin et al. 2007), and consistent with the period distribution among similarly young stars (Figure 8). The uncertainties we quote for the rotation period reflect a measurement error and do not account for differential rotation, which can be as large as 0.2 radian day^{-1} for pre-main sequence stars (Waite et al. 2011). The amplitude of brightness modulations is seen to evolve throughout the *K2* observation period. Such an effect may be observed when two signals with different periods give rise to a beat pattern, which may be due to surface differential rotation, star spot emergence and decay, or two stars contained within the photometric aperture.

V1298 Tau exhibits excess ultraviolet (UV) emission, a common characteristic of similarly young stars. Using data from the *GALEX* mission, Findeisen & Hillenbrand (2010) found a far-UV excess of 3.4 ± 0.7 mag (at 4.7σ significance) and a near-UV excess of 0.8 ± 0.3 mag (2.2σ). The level of UV excess exhibited by V1298 Tau is consistent with members of a similar color in the Lower Centaurus-Crux and Upper Centaurus-Lupus associations (15-25 Myr), while lower than members of the Upper Scorpius OB association (5-10 Myr) and higher than the *Kepler* sample (Olmedo et al. 2015, see Figure 9).

From the *ROSAT* X-ray flux ($f_X = 1.64 \times 10^{-15}$ W m^{-2}), a published MEKAL plasma fit, and hydrogren column density (Boller et al. 2016), we estimate an X-ray
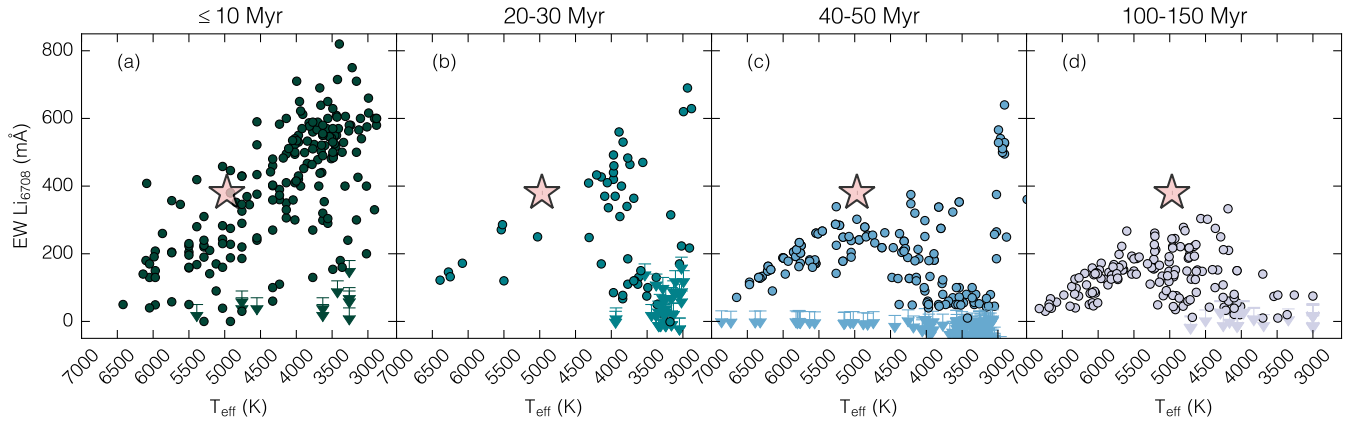
Figure 6. Lithium depletion in young associations. Relationship between effective temperature and Li 6708 Å equivalent width for members of various young associations, moving groups, and clusters. V1298 Tau (pink star) shown for comparison. *(a)* Taurus-Auriga, η Chamaeleontis, and TW Hydrae. *(b)* β Pictoris moving group and NGC 1960. *(c)* Tucanae-Horologium, Carina, Columba, IC2602, and IC2391. *(d)* Pleiades and AB Doradus moving group.
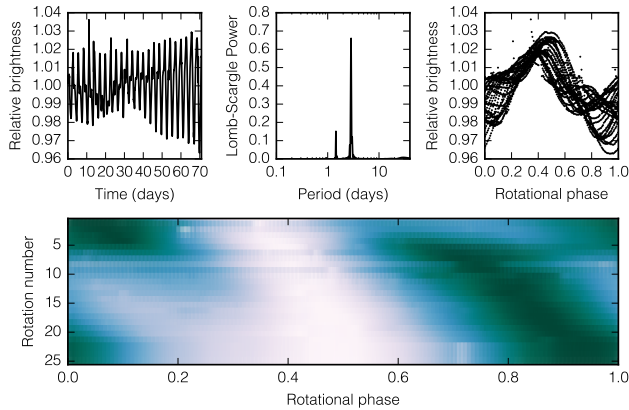
Figure 7. Stellar rotation period. *Top:* from left to right, the full *K2* light curve of V1298 Tau, a Lomb-Scargle periodogram of the *K2* time series photometry with peak power at 2.85 days and a secondary peak at the second harmonic, and the *K2* photometry phased on the rotation period. *Bottom:* Waterfall diagram visualization of the brightness evolution of V1298 Tau throughout the *K2* campaign.

luminosity of $log_{10}(L_X/\text{erg s}^{-1}) = 30.37$, corresponding to a fractional X-ray luminosity of $log_{10}(L_X/L_{\text{bol}}) = -3.22$. The X-ray luminosity of V1298 Tau is essentially consistent with that of a saturated X-ray emitter (Wright et al. 2011) and similar to that for other pre-main sequence fast-rotating stars. The predicted X-ray flux may also be calculated from the Rossby number, $Ro = P_{\text{rot}}/\tau_c$, where τ_c is the convective turnover time. For V1298 Tau, $Ro = 0.173$, where $\tau_c = 16.518$ days was calculated from the $(V - K_s)_0$ color (Wright et al. 2011). From empirical relations (Wright et al. 2011), which suggest V1298 Tau is just below the saturated regime, the predicted fractional X-ray luminosity is $log_{10}(L_X/L_{\text{bol}}) = -3.47$. Using both the measured
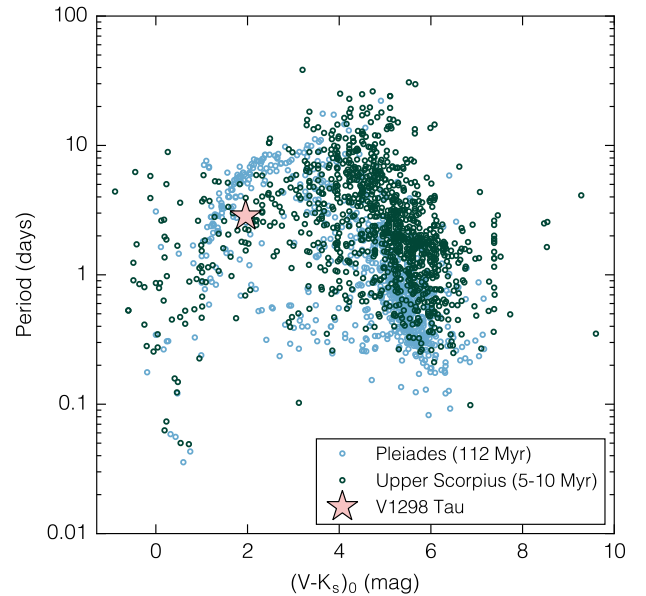
Figure 8. Relationship between colors and variability periods for members of the Upper Scorpius OB association (dark green) and the Pleiades open cluster (light blue), with V1298 Tau (pink star) shown for comparison. Note, the shortest periods at the blue end are due to pulsations rather than surface rotation. Data originate from Rebull et al. (2016, 2018).

and predicted $log_{10}(L_X/L_{\text{bol}})$ values, the age of V1298 Tau implied by an empirical X-ray-age relation (Mamajek & Hillenbrand 2008) is 12–24 Myr, consistent with the age found in a Hertzprsung-Russell diagram.

3.4. *Transit model fitting*

We fit Mandel & Agol (2002) analytic transit models to the *K2* photometry using a combination of

Table 2. System properties of V1298 Tau

Parameter	Value
Stellar properties	
Designations	EPIC 210818897, [WKS96] 4, RX J0405.3+2009
Right ascension (J2000.0)	$04^{\mathrm{h}}05^{\mathrm{m}}19.6^{\mathrm{s}}$
Declination (J2000.0)	$+20°09'25.6"$
Parallax, ϖ (mas)	9.214 ± 0.059
Proper motion R.A., μ_α (mas yr^{-1})	5.23 ± 0.13
Proper motion Dec., μ_δ (mas yr^{-1})	-16.077 ± 0.048
Distance (pc)	108.5 ± 0.7
Spectral type	K0–K1.5
Stellar age, $\tau_\star$ (Myr)	23 ± 4
Stellar mass, $M_\star$ ($M_\odot$)	1.10 ± 0.05
Stellar radius, $R_\star$ ($R_\odot$)	1.305 ± 0.070
Effective temperature, T_{eff} (K)	4970 ± 120
Luminosity, L_* ($L_\odot$)	0.934 ± 0.044
Mean stellar density, $\rho_\star$ (g cm^{-3})	0.697 ± 0.075
Surface gravity, $\log g_\star$ (dex)	4.246 ± 0.034
Stellar rotation period, P_{rot} (d)	2.851 ± 0.050
Projected rotational velocity, vsini (km s^{-1})	23 ± 2
Barycentric radial velocity, γ (km s^{-1})	16.15 ± 0.38
Li I 6708Å equivalent width (mÅ)	380
(B-V) color excess, $E(B-V)$ (mag)	0.024 ± 0.015
J-band extinction, A_{J} (mag)	0.019 ± 0.010
Light curve modeling parameters	
Orbital period (days)	$24.13889^{+0.00043}_{-0.00044}$
Time of mid-transit, t_0 (BJD$_{\mathrm{TDB}}$; days)	$2457091.18842^{+0.00039}_{-0.00038}$
Full transit duration, T_{14} (hours)	$6.386^{+0.048}_{-0.034}$
Total transit duration, T_{23} (hours)	$5.486^{+0.039}_{-0.072}$
Planet-to-star radius ratio, R_p/R_*	$0.07111^{+0.00117}_{-0.00061}$
Scaled semi-major axis, $a/R_\star$	$28.7^{+1.5}_{-2.3}$
Impact parameter, b	$0.23^{+0.16}_{-0.15}$
Cosine of inclination, $\cos i$	$0.0086^{+0.0067}_{-0.0058}$
Inclination, i (deg)	$89.51^{+0.33}_{-0.38}$
Eccentricity, e	$0.087^{+0.216}_{-0.062}$
Longitude of periastron, ω (deg)	92^{+71}_{-72}
Mean stellar density, ρ_* (g cm^{-3})	$0.69^{+0.20}_{-0.26}$
Planet properties	
Planet radius, R_p (R_{Jup})	$0.904^{+0.053}_{-0.048}$
Planet mass, M_p (M_{Jup})	<8.3
Semi-major axis, a (AU)	$0.1688^{+0.0025}_{-0.0026}$
Blackbody equilibrium temperature, T_{eq} (K)	601^{+29}_{-22}

NOTE—Astrometric parameters originate from *Gaia*. Quoted transit parameters and uncertainties are medians and 15.87%, 84.13% percentiles of the posterior distributions.
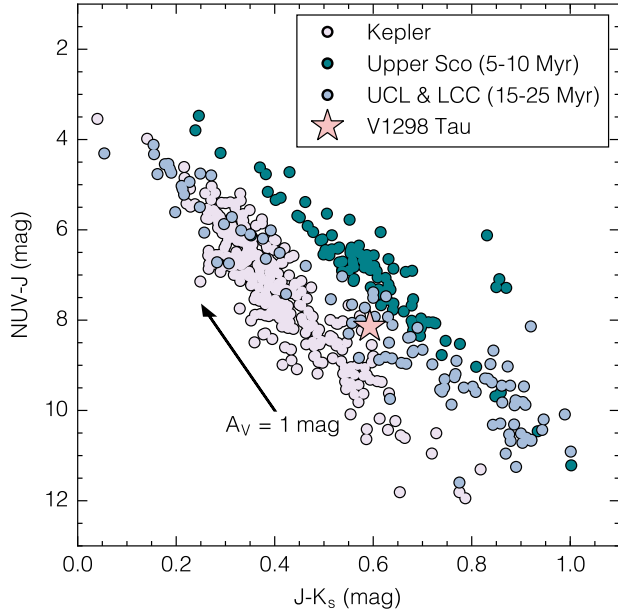
Figure 9. Near-UV and infrared color-color diagram. V1298 Tau exhibits excess UV emission, consistent with similarly young (15-25 Myr) stars in Upper Centaurus-Lupus (UCL) and Lower Centaurus-Crux (LCC), but at a lower level than stars in Upper Scorpius (5-10 Myr). The *Kepler* sample is shown for comparison. The photometry have not been corrected for extinction. A reddening vector is shown for reference. Photometry originate from 2MASS (Skrutskie et al. 2006) and *GALEX* (Martin et al. 2005).

the PYTRANSIT package (Parviainen 2015) and EM-CEE, a Python implementation of the affine invariant Markov chain Monte Carlo (MCMC) ensemble sampler (Foreman-Mackey et al. 2013; Goodman & Weare 2010). The transit model parameters sampled were the orbital period (P), the time of mid-transit (T_0), the planet-to-star radius ratio (R_P/R_*), the scaled semi-major axis (a/R_*), and the cosine of the inclination $(\cos i)$, and two parameter combinations of the eccentricity and longitude of periastron, $(\sqrt{e}\cos\omega,\ \sqrt{e}\sin\omega)$.

We assumed a quadratic limb darkening law, imposing Gaussian priors on the linear and quadratic coefficients. The centers and widths of the limb darkening coefficient priors $(u_1 = 0.621 \pm 0.023,\ u_2 = 0.103 \pm 0.015)$ were determined from tabulated values appropriate for the temperature and surface gravity of V1298 Tau (Claret et al. 2012, 2013). Using an approximate formula for the mean stellar density in the case of eccentric orbits (Kipping 2010), we additionally applied a Gaussian prior on the mean stellar density with a center and width of 0.697 g cm^{-3} and 0.225 g cm^{-3}, respectively. Model transit profiles were numerically integrated to match the

1766 second cadence of the *K2* observations. The target probability density sampled was therefore,

$$\ln\mathcal{L} = -\frac{1}{2}\chi^2 - \frac{1}{2}\frac{(\rho_\star - \mu_{\rho_\star})^2}{\sigma^2_{\rho_\star}}$$
$$-\frac{1}{2}\frac{(u_1 - \mu_{u_1})^2}{\sigma^2_{u_1}} - \frac{1}{2}\frac{(u_2 - \mu_{u_2})^2}{\sigma^2_{u_2}}, \quad (1)$$

where the first term describes the likelihood and the last three terms describe the priors on the mean stellar density and limb darkening parameters.

Convergence was assessed iteratively until the following criteria were met for each directly sampled parameter: (1) the chain length exceeded 50 times the autocorrelation length, and (2) the autocorrelation length estimate changed by <2% from the prior iteration. We discarded the first $10 \times \langle\tau_{\rm acor}\rangle$ steps as burn-in, where $\langle\tau_{\rm acor}\rangle$ is the average autocorrelation length across all parameters. In addition to the fit described above, we performed a circular orbit fit with no prior directly applied to the mean stellar density. This secondary fit was used in an analysis of the host star's evolutionary stage. The results of the transit modeling and derived planet parameters are summarized in Table 2.

As mentioned earlier, several in-transit observations are outliers with no easily discernible nature (i.e., these observations are not obviously affected by spacecraft systematics). Most of these outliers serve to diminish the transit depth. To determine the effect of the outlying observations on the inferred planetary radius we performed transit fits that both included and excluded these outliers. We adopt the fit which excludes the putative spot-crossing events because the scatter about the lower envelope of the transit profile is smaller. When including all observations, the inferred planet size is 1σ smaller than our adopted value $(R_P = 0.86 \pm 0.05\ R_{\rm Jup})$. Future observations in the infrared, where the amplitude of stellar variability is smaller, may measure the planetary radius more securely.

An unassociated star to the southwest of V1298 Tau is partially contained within the *K2* photometric aperture (Figure 10). We show in § 3.10 that this star is not responsible for the transits, but we consider here the effect of flux dilution on the inferred planet radius. In the presence of light from another star, the ratio of the true planet radius to the observed planet radius is given by $R_{\rm P,true}/R_{\rm P,obs} = \sqrt{1 + F_2/F_1}$, where F_2/F_1 is the optical flux ratio between the two stars (Ciardi et al. 2015). The nearby star is 6.3 magnitudes fainter than V1298 Tau in the *Kepler* bandpass, and thus impacts the planet radius by <0.2%, which is much smaller than the stellar radius uncertainty.
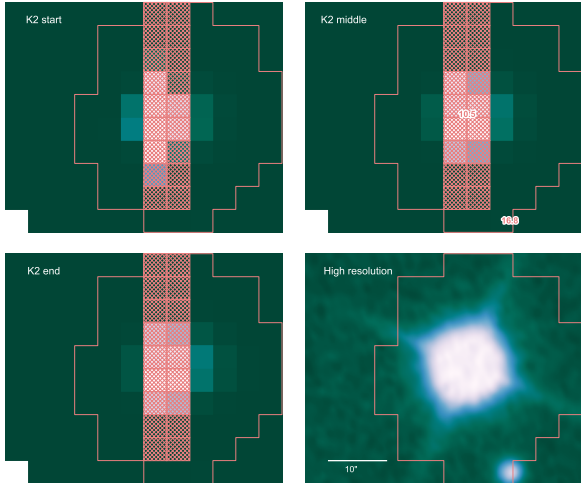
Figure 10. *K2* photometric aperture for V1298 Tau. *K2* target pixel files for V1298 Tau at the start (*top left*), middle (*top right*), and end (*bottom left*) of Campaign 4. *Bottom right:* High resolution image from the Palomar Observatory Sky Survey showing a faint background source to the southwest. The photometric aperture boundary is indicated in pink, with saturated columns shown as hatched regions.

For planets with ingress and egress durations that are sufficiently resolved in time, the eccentricity can be derived from MCMC sampling and a loose stellar density prior (Dawson & Johnson 2012). From the transit fit, we find the marginalized posterior density in eccentricity places limits of $e < 0.16, 0.51, 0.71$ at 68.3%, 95.5%, and 99.7% confidence, respectively (Figure 11). While transit-derived eccentricities can be robust, we stress that radial velocity monitoring or secondary eclipse timing is required to constrain the eccentricity with higher precision and confidence.

3.5. *Centroid motion analysis*

Evidence of offsets in the point spread function (PSF) centroid during transit are indicative of a transit occurring due to a contaminant or background star with a transient nature (e.g. a background eclipsing binary, Thompson et al. 2018). Based on a simple centroiding test, accounting for the *K2* roll motion, the PSF centroids during the expected transit of V1298 Tau b are consistent at the $\lesssim 1\,\sigma$ level with the out of transit centroids (Figure 12). This suggests that the transit signal is not due to a background eclipsing binary and is consistent with originating from the target star.

3.6. *Limits on companions from the transit shape*

The transit shape constrains the probability of hierarchical triple scenarios in which the observed transit signal is due to an eclipsing binary or transiting planet
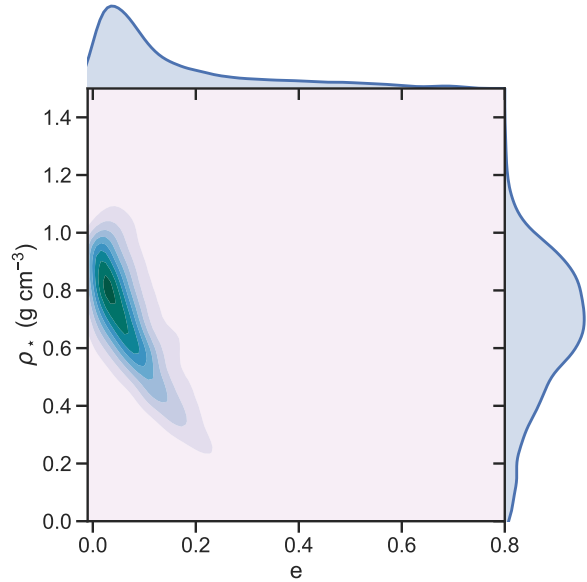
Figure 11. Constraints on eccentricity of V1298 Tau b from the transit fit. Shaded contours show the joint posterior probability densities for the eccentricity of V1298 Tau b and mean stellar density from the transit fit. Marginalized probability densities are shown at top and at right.
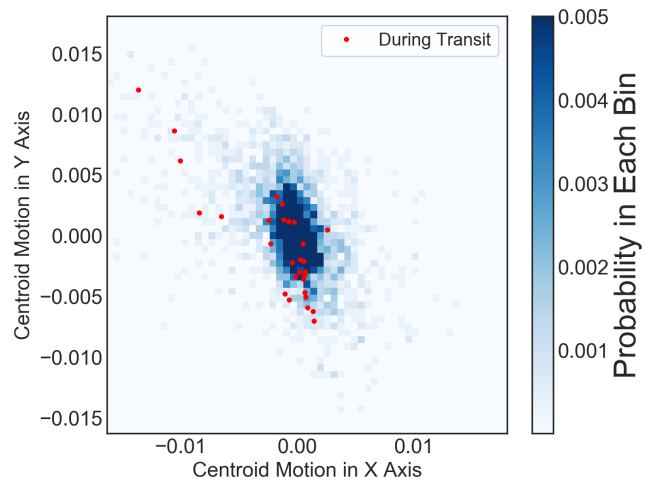
Figure 12. Centroid motion of V1298 Tau. Motion of the point spread function centroid of V1298 Tau throughout the *K2* campaign (two-dimensional histogram). The centroid motions during the transits of V1298 Tau b are shown as red points, and are consistent with with the distribution of out-of-transit centroid shifts at the $\lesssim 1\sigma$ level. The five clear outliers correspond to observations which occurred immediately after a loss of fine-pointing by the telescope.

host which is distinct from, but gravitationally bound to, V1298 Tau. In such scenarios, the flux dilution from V1298 Tau itself requires larger radius ratios (and thus more V-shaped eclipses) between the eclipsing companions in order to reproduce the observed transit depth. To estimate the relative likelihood of these scenarios, we performed Levenberg-Marquardt least-squares fits (with free parameters R_P/R_*, a/R_*, $\cos i$) to the transit profile over a grid of assumed optical contrasts between V1298 Tau and the putative eclipsing companions.

In this case the model time series is given by the equation,

$$f_{\rm dil}(t) = \frac{f(t) + F_1/F_2}{1 + F_1/F_2}, \qquad (2)$$

where $f(t)$ is the normalized eclipse time series in the absence of dilution and F_1/F_2 is the flux ratio between the primary star and the eclipsing companions.

For each contrast value and best-fit eclipse profile, we recorded the χ^2 value. Using the Akaike Information Criterion (AIC) we then evaluated the relative likelihoods of models which assume dilution from the primary star. We found that a model with a companion contrast of $\Delta{\rm mag} = 1$ is 5.6×10^{-4} times as likely as one with $\Delta{\rm mag} = 0$. By comparison, a model assuming dilution from an equal-brightness companion is found to be 0.057 times as likely as the best fit model assuming no additional companion. We also performed an MCMC fit for a diluted transit model, sampling the parameters R_P/R_*, a/R_*, $\cos i$, and $\Delta{\rm mag}$ and using the same convergence criteria utilized in the transit fit described earlier. This analysis leads to a constraint of $\Delta{\rm mag} < 0.76$ for a putative companion at 99.7% confidence. Although the statistical tests described above suggest a stringent limit on the contrast of a putative companion, we adopt a more conservative limit of $\Delta{\rm mag} < 4$, based on the shapes of the best fit transit profiles after accounting for dilution (Figure 13), for plausible hierarchical triple scenarios.

3.7. Limits on companions from imaging

Daemgen et al. (2015) observed V1298 Tau with adaptive optics and the NIRI instrument at Gemini North Observatory on 2011 October 22 11:00 UTC. Those data rule out nearly all scenarios in which V1298 Tau hosts a stellar mass companion with a projected separation of 10.85–1085 AU, where we have interpolated between a 20 Myr isochrone to convert near-infrared contrasts to mass limits (Baraffe et al. 2015). In the time between those observations and our NIRC2 imaging, V1298 Tau moved by 0.120 ± 0.062 arcseconds on the sky due to its proper motion. Combining the two epochs of imaging
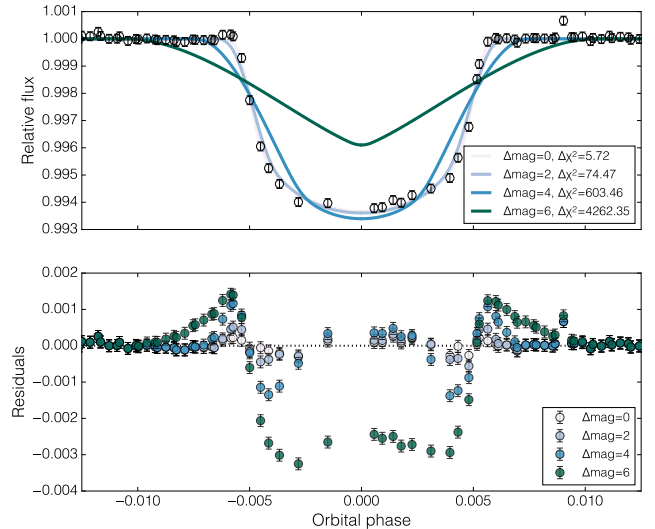

Figure 13. Constraints on companions to V1298 Tau from the transit shape. Best fit transit models after accounting for dilution from V1298 Tau. For large optical contrasts between V1298 Tau and a putative companion, models can not reproduce the observed transit shape and depth. For each assumed contrast, the $\Delta\chi^2$ value between the hierarchical triple model and the single star model is indicated. Scenarios involving a companion with $\Delta{\rm mag} > 4$ are ruled out.

constraints we rule out a vast swath of parameter space involving a background or foreground eclipsing binary that would have been aligned by chance with V1298 Tau during the *K2* observations (Figure 14).

We used a galactic structure model (Girardi et al. 2012) to simulate a 1-deg^2 field centered on V1298 Tau in order to estimate the number of foreground or background stars in the region of parameter space not excluded by our observations. We found that 0.004 sources with $3.4 < \Delta V < 5.8$ mag are expected in the surrounding $0.1'' \times 0.1''$ region. An even smaller number of sources are expected to be eclipsing binaries.

3.8. Limits on companions from spectroscopy

We used a 24-year radial velocity time series (Wichmann et al. 2000; Nguyen et al. 2012, this work), including our newly acquired data, to search for bound companions to V1298 Tau. We assumed an uncertainty of 1 km s^{-1} for each observed radial velocity to allow for the possibility of zero-point offsets between different instruments or other systematic biases. At each point in a grid of orbital period and companion mass we simulated 1000 circular spectroscopic binary orbits, sampled at the times of the observations. For each simulated orbit, the inclination was drawn randomly from a uniform distribution in $\cos i$ and the phase was drawn randomly from a uniform distribution between $[0,2\pi]$. To simulate radial velocity jitter, we added Gaussian noise with an
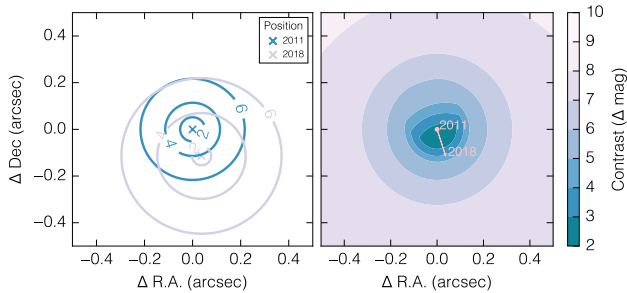
Figure 14. Multi-epoch adaptive optics imaging of V1298 Tau. *Left:* Radial contrast contours in the 1" region surrounding V1298 Tau from multi-epoch adaptive optics imaging. *Right:* Combination of the individual constraints results in a minimum contrast of ΔK=2.1 mag everywhere in the surrounding region, including behind the position of V1298 Tau during the *K2* observations.
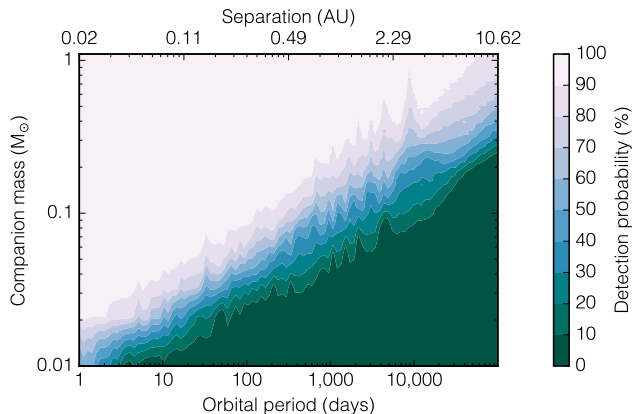
Figure 15. Radial velocity limits on companions to V1298 Tau. Detection probability in the period-companion mass plane for simulated spectroscopic binaries given the 24 year radial velocity time series. The axis at top indicates the physical separation for a 0.5 M$_\odot$ companion. The 95% detection probability contour is depicted in Figure 16.

amplitude of 200 m s^{-1} to each model. At each point in the period-companion mass plane we then determined the detection probability as the fraction of successfully detected simulated orbits. An individual simulated orbit was considered successfully detected if the $\Delta\chi^2$ value between the simulated radial velocities and the null hypothesis of constant velocity exceeded 20. From this analysis we are able to rule out a wide range of brown dwarf and stellar companions with orbital periods between 1–10,000 days (Figure 15).

In a search for secondary spectral lines in the HIRES spectrum (Kolbl et al. 2015) we found no stars brighter than 5% the brightness of the primary and with a projected separation of ≤0".4. We note that this search is only sensitive to stars with radial velocity separa-

tions >50 km s^{-1} (corresponding approximately to two linewidths of V1298 Tau), as the two sets of spectral lines would otherwise be indistinguishable.

3.9. *Limits on companions from astrometry*

Gaia resolves double stars, either associated or unassociated, outside of 1″ down to optical contrasts of 6 magnitudes and irrespective of a companion's position angle (Ziegler et al. 2018). Only one other star was detected by *Gaia* within the boundaries of the *K2* photometric aperture. We show later that star is too faint to be a false-positive. At smaller separations, the goodness-of-fit of the *Gaia* astrometric solution provides another means of assessing multiplicity. A previous study of exoplanet host stars with closely-projected companions showed that the *Gaia* astrometric fit metrics can be used to reliably detect companions with separations of 0.08–1″ and optical contrasts <2 mag (Rizzuto et al. 2018). Furthermore, exoplanet host stars with detected companions at projected separations of 0.05–1″ typically have astrometric goodness-of-fit values >20 with excess astrometric noise often detected at 5σ significance (Evans 2018). In the case of V1298 Tau, the goodness-of-fit in the along-scan direction is 9.0, with zero detectable excess astrometric noise. While not conclusive, the *Gaia* data suggest V1298 Tau is unlikely to host a stellar companion with a mass above 0.5 M$_\odot$ (corresponding to a model-derived optical contrast of 2 mag at 20 Myr (Baraffe et al. 2015)) and separation greater than 0.08″(8.7 AU).

3.10. *False-positive scenario assessment*

False-positive signals in transit surveys can be due to an eclipsing binary or a planet transiting a star other than the assumed host. We consider each false-positive scenario in detail below (summarized in Figure 16), and conclude that the interpretation of a Jupiter-sized planet transiting V1298 Tau is the one most consistent with observations.

An eclipsing binary can dim by a maximum of 100%, which sets a firm upper limit of 5.7 magnitudes to the optical contrast between V1298 Tau and a putative false-positive capable of reproducing the observed transit depth. Although an unassociated star is included in the target pixel files for V1298 Tau, it is too faint to reproduce the observed transit depth and we recovered the transits from a small photometric aperture excluding that star. Inside of 0.1″, assuming an unassociated eclipsing binary would not be co-moving with V1298 Tau, we effectively ruled out background or foreground stars by leveraging the proper motion of V1298 Tau between two epochs of adaptive optics imaging separated by 6 years. At separations of 0.1–20″, adaptive
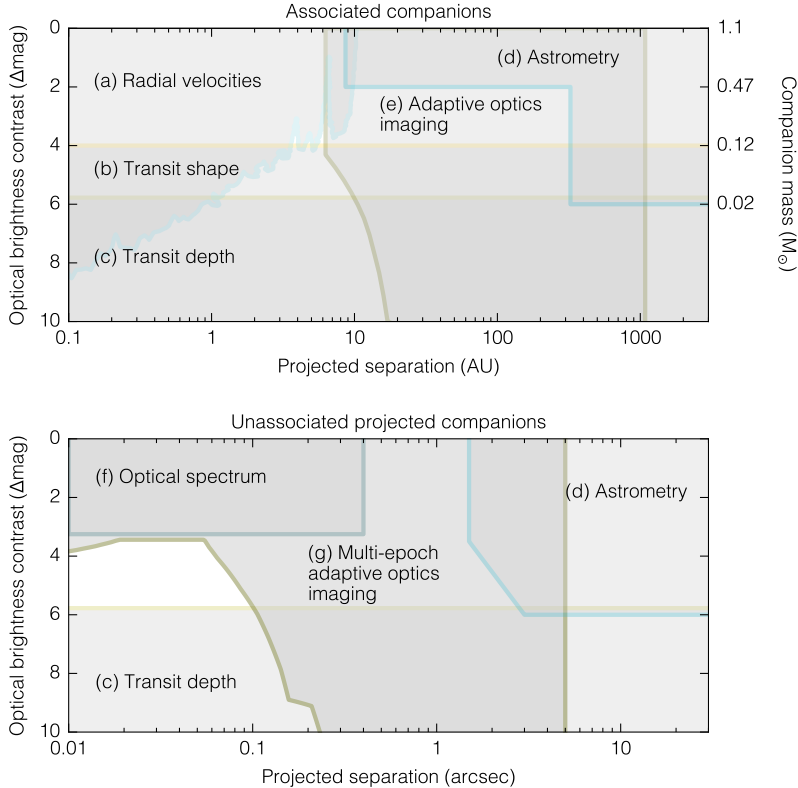
Figure 16. Constraints on astrophysical false-positive scenarios. Regions of the separation-contrast plane excluded by observations are shown for associated companions at top, and unassociated companions below. *(a)* Sustained radial velocity monitoring rules out associated eclipsing binaries at close separations. *(b)* The transit shape rules out certain hierarchical triple scenarios at any separation. *(c)* The observed transit depth sets an upper limit of 5.7 mag to the optical contrast between V1298 Tau and a putative false-positive, whether it be associated or not. *(d) Gaia* astrometry resolves point sources beyond $1''$, while the astrometric goodness-of-fit is a predictor of associated companions outside of 80 mas. *(e)* Adaptive optics imaging rules out wide associated companions. *(f)* A search for secondary spectral lines would have detected bright eclipsing binaries at close separations as long as the velocity separation with V1298 Tau was >50 km s^{-1}. *(g)* Multi-epoch adaptive optics combined with the proper motion of V1298 Tau eliminates the bulk of unassociated false-positive scenarios. The probability of an unassociated eclipsing binary residing within $0.1''$, where our observations are not sensitive, is $<4/1000$.

optics imaging, all-sky photometric surveys, and *Gaia* rule out additional stars bright enough to be a false-positive. Furthermore, a time series analysis of the *K2* point spread function indicates that the centroid shifts during transits are consistent with those signals originating from V1298 Tau.

False-positive scenarios involving hierarchical triples, i.e. an eclipsing binary or a transiting planet host which is gravitationally bound to V1298 Tau, are similarly disfavored. At close separations (<10 AU), we used a 24-year radial velocity time series (Wichmann et al. 2000; Nguyen et al. 2012) to rule out stellar and brown dwarf companions in a mass-dependent manner, allowing for isotropically distributed inclinations of a putative companion. At intermediate separations (~10–1000 AU), previously published (Daemgen et al. 2015) and newly acquired adaptive optics imaging rules out nearly all stellar companions. Furthermore, the lack of astromet-

ric noise detected with *Gaia* suggests there are no companions down to ~0.5 $M_\odot$ in the ~10–300 AU range. At projected separations beyond 1000 AU, stellar mass and some brown dwarf companions would have been detected by *Gaia* or all-sky surveys. Further discussion of false-positive scenarios is presented in Appendix A.

3.11. *Limit on the planet mass*

Using the RADVEL radial velocity orbit fitting code (Fulton et al. 2018), we fit the PRV measurements of V1298 Tau in order to find an upper limit to the planet's mass (Figure 17). Due to the sparse orbital phase coverage of our data and to the high radial velocity jitter of the star, this upper limit is very likely to be conservative. We assumed a circular orbit for our fits, imposing Gaussian priors on the period and time of inferior conjunction corresponding to the values found from the transit fit (Table 2). Furthermore, the jitter amplitude was
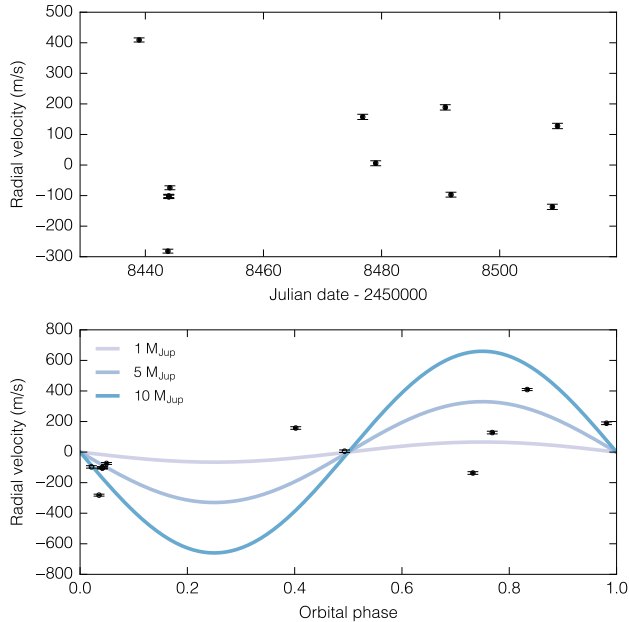
Figure 17. Precision radial velocities of V1298 Tau. *Top:* Keck/HIRES precision radial velocity time series of V1298 Tau. *Bottom:* PRV measurements as a function of orbital phase, with representative circular Keplerian orbits shown for reference.

fixed to 200 m s^{-1}, corresponding approximately to the root mean square dispersion between all measurements. The parameter space defined by the period, time of inferior conjunction, radial velocity semi-amplitude, and velocity zero-point was then explored through MCMC sampling. The resulting posterior of the radial velocity semi-amplitude provides a 3σ upper limit to the planet mass of $M_P < 8.3\ M_{\rm Jup}$.

4. DISCUSSION

Without a measurement of the planet's mass, it is difficult to place V1298 Tau b in proper context with respect to the observed exoplanet population. The size of the planet is significantly smaller than the predictions of many evolutionary models for Jovian-mass planets (Burrows et al. 1997; Baraffe et al. 2003; Fortney et al. 2007; Mordasini et al. 2012; Owen & Wu 2013), which predict radii of $\gtrsim 1.3\ R_{\rm Jup}$ at an age of ~ 20 Myr. In fact, the models of Fortney & Nettelmann (2010) suggest that the combination of age, radius, and separation for V1298 Tau b is inconsistent with a gas-dominated composition for a planet with mass $>0.1\ M_{\rm Jup}$ ($32\ M_{\oplus}$). On the other hand, the observed properties of V1298 Tau b might be reproduced by a planet with a core-dominated composition and mass in the range 0.1–0.3 $M_{\rm Jup}$. If the true mass of V1298 Tau b is $\gtrsim 0.3\ M_{\rm Jup}$, it may still be considered a warm Jupiter by conventional definitions.

Relative to hot Jupiters, less is known about warm Jupiters, though similar mechanisms are invoked to explain their origins. There is evidence for two distinct populations of warm Jupiters. The majority of these planets are characterized by low eccentricities ($e \lesssim 0.2$), nearby and coplanar super-Earth companions, and a dearth of external Jovian-mass companions (Dong et al. 2014; Huang et al. 2016). The remaining warm Jupiters are characterized by moderately eccentric ($e \gtrsim 0.4$) orbits, often accompanied by external Jovian-mass companions which are mutually inclined and apsidally misaligned (Dawson & Chiang 2014).

In general, warm Jupiters do not have eccentricities large enough to become hot Jupiters through tidal dissipation (Dawson et al. 2015). Furthermore, population synthesis studies examining the outcomes of various high-eccentricity migration scenarios have struggled to reproduce the observed ratio of hot and warm Jupiters (Antonini et al. 2016; Petrovich & Tremaine 2016). Both of these points of evidence are seen as a major weakness in the high-eccentricity migration hypothesis. However, secular interactions with a neighboring planet could excite the eccentricity of V1298 Tau b at a later stage (Anderson & Lai 2017).

While the transit fit for V1298 Tau b suggests a low to moderate eccentricity, solutions with $e > 0.5$ are not ruled out. However, eccentricities measured from transit photometry (particularly long-cadence *Kepler* data as in this case) should be regarded with caution. Although no additional transiting companions were found, transit injection and recovery simulations would be necessary to quantify the sensitivity of the *K2* data in detail. Until the mass and eccentricity of V1298 Tau b are measured through radial velocities or secondary eclipse timing, it remains unclear whether the planet belongs to either of the known warm Jupiter populations. Even if V1298 Tau b is found to have a moderately low eccentricity, long-term radial velocity monitoring is required to test the hypothesis that the planet might have an external companion that is nearby and massive enough to force episodic tidal migration through secular planet-planet interactions.

5. CONCLUSIONS

We report the detection and validation of a warm Jupiter-sized planet transiting a young solar analog, with an estimated age of 23 million years. The star and its planet belong to a newly characterized association, named Group 29, in the foreground of the Taurus-Auriga star-forming region (Oh et al. 2017; Luhman 2018). Through a detailed analysis of the *K2* data and follow-on observations, we found no evidence for a stel-
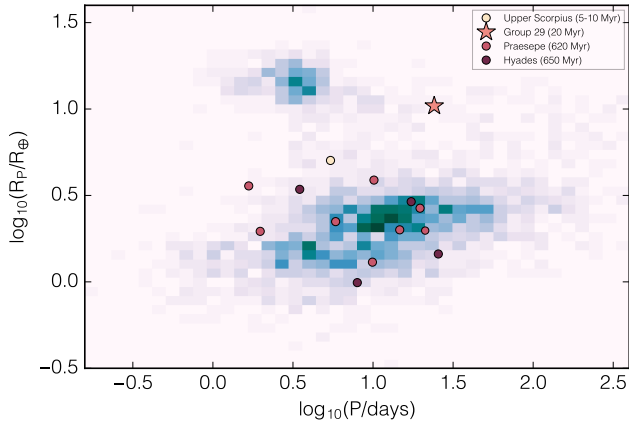
Figure 18. V1298 Tau b (pink star) compared to the sample of confirmed transiting exoplanets (two-dimensional histogram) in the period-radius domain. Transiting planets in young clusters and associations are shown for comparison.

lar companion and we securely ruled out most plausible false-positive scenarios. The young age of the planetary system suggests that it is very unlikely to have reached its current orbit through a high-eccentricity migration channel. More likely, the planet formed *in situ* (e.g. Batygin et al. 2016; Boley et al. 2016) or at a wider separation followed by planet-disk interactions (Kley & Nelson 2012).

The transit profiles exhibit some anomalous features, and it is presently unclear whether the outlying observations are systematic or astrophysical in nature. Transit observations in the infrared, where the amplitude of stellar variability is lower, should yield a more secure measurement of the planet's radius. With finer temporal resolution in ingress and egress, such observations might also lead to tighter constraints on the planet's eccentricity. To measure the planet's mass, it is also preferable to observe in the infrared, as we have measured the optical radial velocity jitter to be $\sim$200 m s^{-1} (compared with the range of predicted Doppler semi-amplitudes of 13–230 m s^{-1}). We discuss the favorability of V1298 Tau for various follow-up observations further in Appendix B.

Although several groups have published candidate exoplanet catalogs encompassing nearly every *K2* campaign, the V1298 Tau system seems to have evaded detection, despite the relatively large transit depth. The most likely explanation seems to be that automated transit search pipelines are not tailored to the high-amplitude, short-timescale variability exhibited by young stars. Customized or more generalized routines which are not susceptible to under- or over-fitting stellar variability are therefore needed to adequately search the light curves of young stars for transiting planets (e.g. Rizzuto et al. 2017).

Presently, there is only one other secure case of an exoplanet transiting a pre-main sequence star: the Neptune-sized planet K2-33 b in the 5 to 10 million-year-old Upper Scorpius OB association (David et al. 2016; Mann et al. 2016b). V1298 Tau b is now the second youngest transiting exoplanet, and the first secure case of a transiting Jovian-sized planet orbiting a pre-main sequence star. Many of the other transiting planets found in young ($<$1 Gyr) clusters reside in low-occurrence regions of the period-radius diagram (Figure 18), such as the radius valley or the sub-Jovian desert. V1298 Tau b seems to follow this trend, though it is as yet unclear whether this planet is a Jovian-mass resident of the "period-valley" (Udry et al. 2003; Santerne et al. 2016), a progenitor of the rare sub-Saturn class (Petigura et al. 2017), or perhaps contracting down to the sub-Neptune "main-sequence."

Software: astropy (Astropy Collaboration et al. 2013), BANYAN Σ (Gagné et al. 2018), emcee (Foreman-Mackey et al. 2013), EVEREST 2.0 (Luger et al. 2018), K2SC (Aigrain et al. 2016), K2PHOT (Petigura et al. 2018), lightkurve (Barentsen et al. 2019), lmfit (Newville et al. 2014), PyTransit (Parviainen 2015), RadVel (Fulton et al. 2018), TERRA (Petigura et al. 2013),

APPENDIX

A. FALSE-POSITIVE SCENARIO ASSESSMENT

An eclipsing binary or a planet transiting a star other than V1298 Tau would be capable of producing the observed transit signal. Below, we assess the likelihood of each possible false-positive scenario in a quantitative manner when possible and qualitatively otherwise.

We first consider a scenario in which the transit signal is due to an unassociated eclipsing binary widely separated from V1298 Tau on the sky. Occasionally, a bright eclipsing binary within the telescope field of view may contaminate pixels elsewhere on the detector and lead to spurious detections of transiting planets. There are several stars, some saturated, in the vicinity of V1298 Tau on the *K2* detector. We examined light curves for each of these stars (EPIC IDs 210819568, 210817793, 210818376) and confirmed that none showed eclipses. We similarly examined light curves for neighboring stars identified using the star.neighbors function with everest 2.0, and found no eclipsing binaries among those stars (EPIC IDs 210787602, 210755820, 210852007, 210832303, 210829398, 210769653, 210828429, 210815489, 210761528).

Our group also performed a systematic search of every *K2* light curve from Campaign 4 (Crossfield et al. 2016) for periodic transits or eclipses using the terra code (Petigura et al. 2013). We used the output of this search to attempt a cross-match between the ephemeris of V1298 Tau with known periodic signals detected by terra above a signal-to-noise of 10. We examined the *K2* light curves for 50 stars having signals detected with periods within 0.5 days of the period of V1298 Tau b or half of that period. We found none of those stars to show eclipses coinciding with the transit times of V1298 Tau b. A search of the *Kepler* Eclipsing Binary Catalog (http://keplerebs.villanova.edu/) for eclipsing binaries discovered from Campaign 4 of the *K2* mission also yielded no candidates with period differences of <0.64 days relative to V1298 Tau b.

Next we consider closely-projected eclipsing binaries that are either associated or unassociated with V1298 Tau. An eclipsing binary can dim by at most 100%. The observed transit depth therefore sets an upper limit to the brightness difference in the *Kepler* bandpass of 5.7 magnitudes between V1298 Tau and a putative eclipsing binary capable of producing the observed transit depths. The target pixel files for V1298 Tau contain an unassociated star, Gaia DR2 51886331671984640, which resides 19.8 arcseconds to the southwest. This star is more than 6 magnitudes fainter than V1298 Tau at optical wavelengths, and therefore too faint to be responsible for the periodic transits. Using the interactive lightkurve[3] tool, we examined time series photometry for V1298 Tau from a 24"×24" square aperture as well as from a 12"×8" rectangular aperture surrounding the fainter source to the southwest. We confirmed that the fainter source is not an eclipsing binary and that the transit signal originates from the region surrounding V1298 Tau.

False-positive scenarios involving hierarchical triples, e.g. a bound eclipsing binary or a planet transiting an undetected companion to V1298 Tau, are similarly disfavored. Nguyen et al. (2012) searched for close companions to V1298 Tau through radial velocity monitoring. Those measurements rule out most scenarios in which V1298 Tau hosts a stellar mass companion with an orbital period between 1–100 days. Furthermore, dynamical stability arguments (Mardling & Aarseth 2001) and empirical evidence from hierarchical multiple star systems (Tokovinin 2018) suggest the ratio of the outer to inner periods in a coplanar hierarchical triple must exceed 4.7. Thus, hierarchical triple scenarios involving a coplanar stellar companion with an orbital period <113 days (∼0.5 AU, ∼5 milliarcseconds) are *a priori* unlikely.

Although hierarchical triple scenarios are considered unlikely, we consider the implications of such scenarios here. If V1298 Tau is in fact a binary and the transiting body orbits the primary star, the effect of flux dilution is then maximized when the undetected companion is equal in brightness. In such a scenario, the planet's true radius is larger by a factor of $\sqrt{2}$, corresponding to a radius for the transiting companion of 1.3 $R_{\rm Jup}$ (Ciardi et al. 2015). Notably, such a scenario would still favor a planetary nature for the transiting companion given that low-mass stars and brown dwarfs have radii $\gtrsim$2 $R_{\rm Jup}$ at ages <40 Myr. However, if the transiting body instead orbits an undetected companion

---

[3] http://docs.lightkurve.org
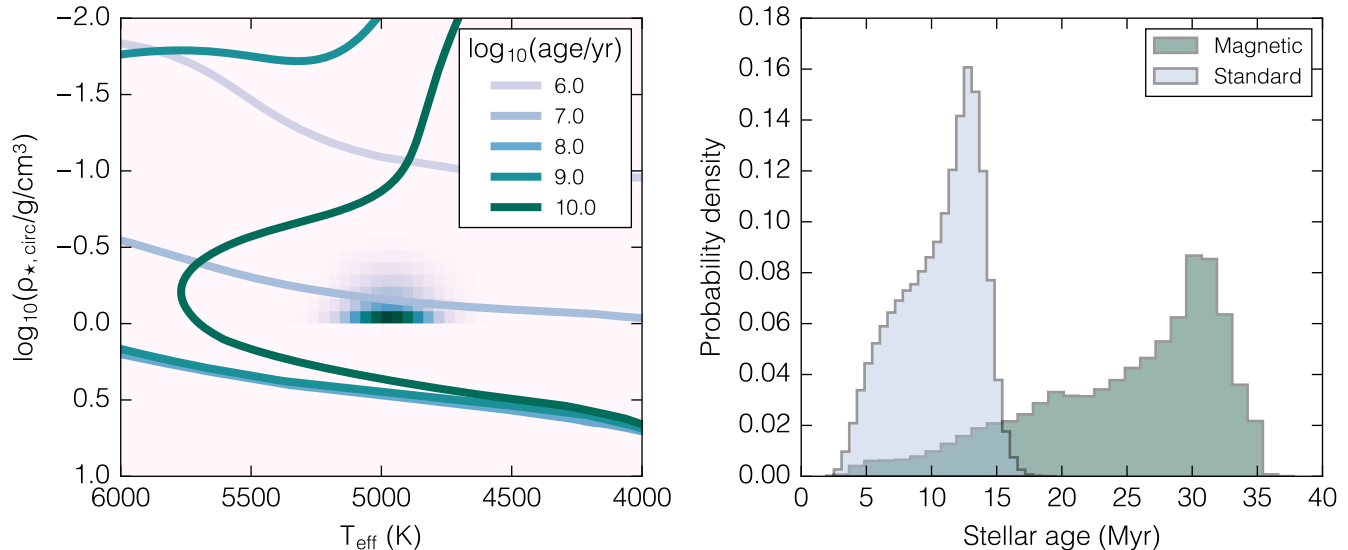
Figure 19. Age inference in a temperature-density diagram. *Left:* The mean stellar density as a function of effective temperature varies with age (solid lines). The two-dimensional histogram shows a normal distribution in temperature and the mean stellar density posterior from the V1298 Tau b transit fit assuming a circular orbit. *Right:* The probability distributions in age for V1298 Tau resulting from a linear interpolation of the values at left using two different evolutionary models (Dotter et al. 2008; Feiden 2016).

star, then the radius is most severely underestimated when the optical contrast between a putative companion and V1298 Tau is maximized. Using evolutionary models and previously established methods (David et al. 2016), we calculated the corrected companion radius and mass in such scenarios, finding that the mass of the transiting body could exceed 0.1 $M_\odot$ if V1298 Tau hosts an undetected companion of 0.5 $M_\odot$ or lower.

The mean stellar density measured from the transits provides another means of assessing false-positive scenarios. Using the posteriors in period and a/R_* from a circular orbit fit, we calculated the mean stellar density and compared it to stellar evolution models in a temperature-density diagram (Figure 19). Although this analysis assumes a circular orbit and should thus be regarded with caution, we find the stellar age implied by the density posterior is consistent with our Hertzsprung-Russell diagram analysis and inconsistent with a main sequence star or a post-main sequence star of similar effective temperature and with an age less than the age of the universe.

B. FAVORABILITY FOR FOLLOW-UP OBSERVATIONS

We compared V1298 Tau b with the population of confirmed transiting exoplanets using data from the NASA Exoplanet Archive (Akeson et al. 2013), accessed on February 20, 2019. We first compared the favorability for atmospheric characterization between V1298 Tau b and known transiting planets. We followed the methods of Vanderburg et al. (2016) to predict a scaled signal-to-noise for transmission spectroscopy observations using the following equations:

$$S/N \propto \frac{R_P H \sqrt{F t_{14}}}{R_\star^2} \tag{B1}$$

and

$$H = \frac{k_B T_{eq}}{\mu g}, \tag{B2}$$

where R_P and $R_\star$ are the radii of the planet and star, respectively, H is the atmospheric scale height, F is the stellar flux at H-band, t_{14} is the total transit duration, k_B is Boltzmann's constant, T_{eq} is the planet's equilibrium temperature, μ is the mean molecular weight of the planet's atmosphere, and g is the planet's surface gravity. When
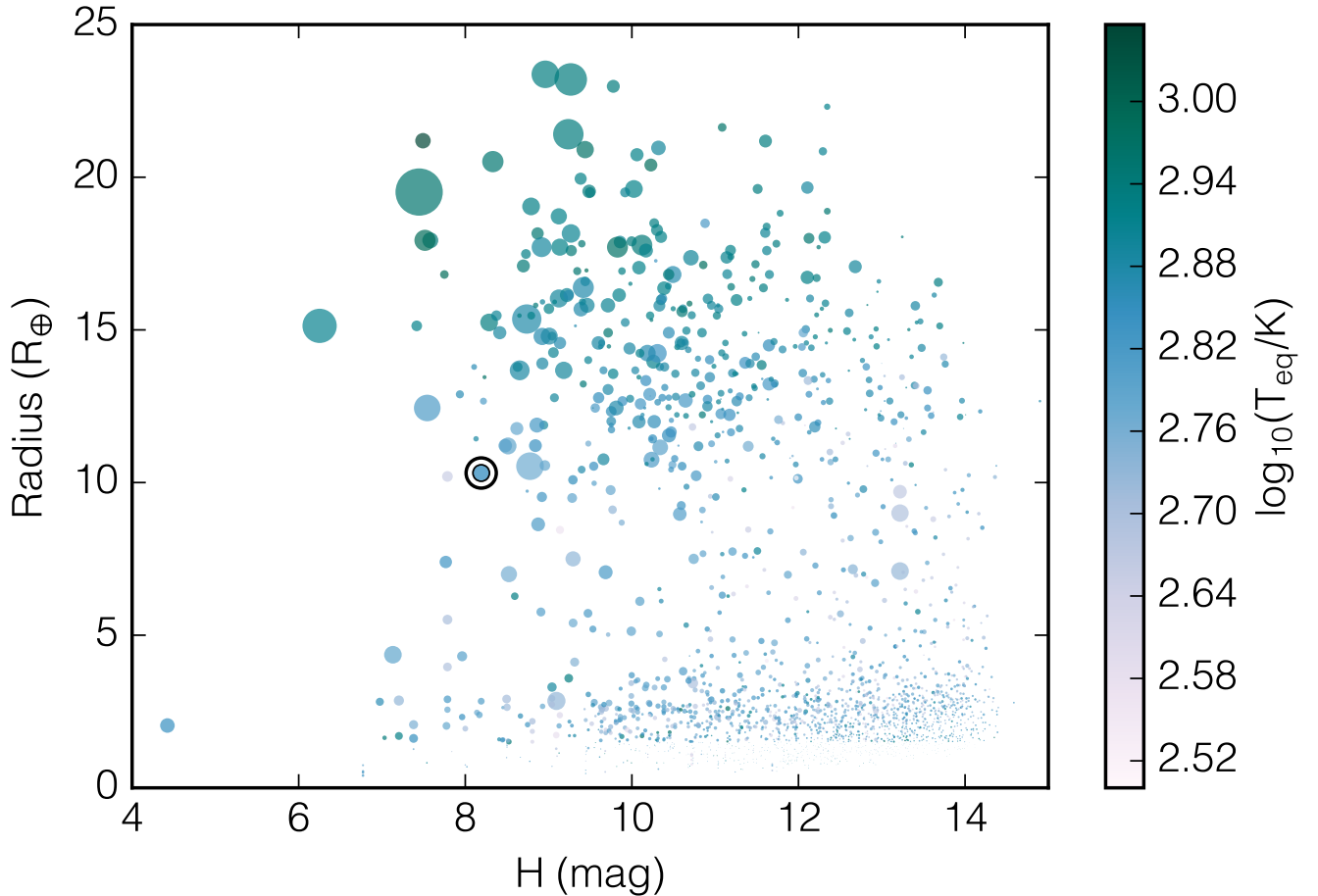
Figure 20. Favorability for transmission spectroscopy. The distribution of known transiting exoplanets as a function of H-band brightness and planet radius. The point size is proportional to the scaled signal-to-noise predicted for transmission spectroscopy observations. Point colors indicate the logarithm of the planet equilibrium temperature, assuming an albedo of 0.3. V1298 Tau b is shown as the point with the black border. The thin and thick borders represents cases of $M_P = 100\ M_\oplus$ and $30\ M_\oplus$, respectively.

available, we used the known mass and radius to calculate surface gravity. Otherwise, we calculated a predicted mass using the planet's radius and an exoplanet mass-radius relation (Weiss et al. 2018). The mean molecular weight was fixed to the Jovian value for planets with radii larger than 1.5 $R_\oplus$ and to the terrestrial value otherwise.

The scaled transmission spectrum signal-to-noise as a function of H-band brightness, planet radius, and equilibrium temperature is depicted in Figure 20. Using this simplistic methodology, we determined that V1298 Tau b ranks among the top 40 most favorable transiting exoplanets for atmospheric characterization. However, in the optimistic case that the planet in fact has a core-dominated composition with a total mass of 30 $M_\oplus$, V1298 Tau b would be in the top 5 in terms of favorability for infrared transmission spectroscopy using the metrics described. Of course, the unusually high stellar activity presents both challenges (potentially requiring multiple transit observations to disentangle stellar and planetary signals) and opportunities (for studying star-planet interactions).

There are presently 16 known exoplanets with radii $> 0.8\ R_{\rm Jup}$, periods between 10–50 days, and well-measured masses $< 10\ M_{\rm Jup}$. Those planets have masses ranging from 0.2–3.5 $M_{\rm Jup}$. For this range of plausible planet masses, the expected radial velocity semi-amplitude ranges from 13–230 m s^{-1}. If V1298 Tau b is contracting, implying its present-day radius may be an imprecise indicator of its mass, the true radial velocity amplitude may be lower. We have measured the optical radial velocity jitter to be $\sigma_{RV} = 216$, 71, and 5 m s^{-1} over 5.2 days, 10 hours, and 30 minutes, respectively. Measuring the planet's mass may be feasible with newly commissioned infrared spectrographs, due to the lower expected intrinsic stellar variability at redder wavelengths.

V1298 Tau is also a favorable target for measuring the planet's obliquity through the Rossiter-McLaughlin (R-M) effect or Doppler tomography. Neglecting limb darkening effects, the R-M amplitude is approximately $A_{RM} \sim v \sin i \times (R_P/R_\star)^2 \times \sqrt{1 - b^2}$, which is 117 m s^{-1} for V1298 Tau. Assuming an albedo of 0.3 and neglecting remnant heat from the planet's formation, the predicted secondary eclipse depth is $\delta_{SE} = (R_P/R_\star)^2 \, (T_{eq}/T_\star) \approx 610$ ppm, which is detectable with the *Spitzer* space telescope. A measurement of the temperature of V1298 Tau b could help to constrain planet evolution models.

REFERENCES

Aigrain, S., Parviainen, H., & Pope, B. J. S. 2016, MNRAS, 459, 2408, doi: 10.1093/mnras/stw706

Akeson, R. L., Chen, X., Ciardi, D., et al. 2013, PASP, 125, 989, doi: 10.1086/672273

Anderson, K. R., & Lai, D. 2017, MNRAS, 472, 3692, doi: 10.1093/mnras/stx2250

Antonini, F., Hamers, A. S., & Lithwick, Y. 2016, AJ, 152, 174, doi: 10.3847/0004-6256/152/6/174

Astropy Collaboration, Robitaille, T. P., Tollerud, E. J., et al. 2013, A&A, 558, A33, doi: 10.1051/0004-6361/201322068

Baraffe, I., Chabrier, G., Barman, T. S., Allard, F., & Hauschildt, P. H. 2003, A&A, 402, 701, doi: 10.1051/0004-6361:20030252

Baraffe, I., Homeier, D., Allard, F., & Chabrier, G. 2015, A&A, 577, A42, doi: 10.1051/0004-6361/201425481

Barentsen, G., Hedges, C., Vincius, Z., et al. 2019, KeplerGO/lightkurve: Lightkurve v1.0b29, doi: 10.5281/zenodo.2565212. https://doi.org/10.5281/zenodo.2565212

Barrado y Navascués, D., Deliyannis, C. P., & Stauffer, J. R. 2001, ApJ, 549, 452, doi: 10.1086/319045

Batygin, K., Bodenheimer, P. H., & Laughlin, G. P. 2016, ApJ, 829, 114, doi: 10.3847/0004-637X/829/2/114

Binks, A. S., & Jeffries, R. D. 2014, MNRAS, 438, L11, doi: 10.1093/mnrasl/slt141

Boley, A. C., Granados Contreras, A. P., & Gladman, B. 2016, ApJL, 817, L17, doi: 10.3847/2041-8205/817/2/L17

Boller, T., Freyberg, M. J., Trümper, J., et al. 2016, A&A, 588, A103, doi: 10.1051/0004-6361/201525648

Bouvier, J., Barrado, D., Moraux, E., et al. 2018, A&A, 613, A63, doi: 10.1051/0004-6361/201731881

Bowler, B. P. 2016, PASP, 128, 102001, doi: 10.1088/1538-3873/128/968/102001

Burrows, A., Marley, M., Hubbard, W. B., et al. 1997, ApJ, 491, 856, doi: 10.1086/305002

Capitanio, L., Lallement, R., Vergely, J. L., Elyajouri, M., & Monreal-Ibero, A. 2017, A&A, 606, A65, doi: 10.1051/0004-6361/201730831

Ciardi, D. R., Beichman, C. A., Horch, E. P., & Howell, S. B. 2015, ApJ, 805, 16, doi: 10.1088/0004-637X/805/1/16

Ciardi, D. R., Crossfield, I. J. M., Feinstein, A. D., et al. 2018, AJ, 155, 10, doi: 10.3847/1538-3881/aa9921

Claret, A., Hauschildt, P. H., & Witte, S. 2012, A&A, 546, A14, doi: 10.1051/0004-6361/201219849

—. 2013, A&A, 552, A16, doi: 10.1051/0004-6361/201220942

Crossfield, I. J. M., Ciardi, D. R., Petigura, E. A., et al. 2016, ApJS, 226, 7, doi: 10.3847/0067-0049/226/1/7

Curtis, J. L., Vanderburg, A., Torres, G., et al. 2018, AJ, 155, 173, doi: 10.3847/1538-3881/aab49c

Daemgen, S., Bonavita, M., Jayawardhana, R., Lafrenière, D., & Janson, M. 2015, ApJ, 799, 155, doi: 10.1088/0004-637X/799/2/155

David, T. J., Hillenbrand, L. A., Petigura, E. A., et al. 2016, Nature, 534, 658, doi: 10.1038/nature18293

Davies, C. L., Gregory, S. G., & Greaves, J. S. 2014, MNRAS, 444, 1157, doi: 10.1093/mnras/stu1488

Dawson, R. I., & Chiang, E. 2014, Science, 346, 212, doi: 10.1126/science.1256943

Dawson, R. I., & Johnson, J. A. 2012, ApJ, 756, 122, doi: 10.1088/0004-637X/756/2/122

Dawson, R. I., Murray-Clay, R. A., & Johnson, J. A. 2015, ApJ, 798, 66, doi: 10.1088/0004-637X/798/2/66

Deming, D., Wilkins, A., McCullough, P., et al. 2013, ApJ, 774, 95, doi: 10.1088/0004-637X/774/2/95

Dobashi, K., Uehara, H., Kandori, R., et al. 2005, PASJ, 57, S1, doi: 10.1093/pasj/57.sp1.S1

Donati, J. F., Moutou, C., Malo, L., et al. 2016, Nature, 534, 662, doi: 10.1038/nature18305

Dong, S., Katz, B., & Socrates, A. 2014, ApJL, 781, L5, doi: 10.1088/2041-8205/781/1/L5

Dotter, A., Chaboyer, B., Jevremović, D., et al. 2008, ApJS, 178, 89, doi: 10.1086/589654

Evans, D. F. 2018, Research Notes of the American Astronomical Society, 2, 20, doi: 10.3847/2515-5172/aac173

Feiden, G. A. 2016, A&A, 593, A99, doi: 10.1051/0004-6361/201527613

Findeisen, K., & Hillenbrand, L. 2010, AJ, 139, 1338,
    doi: 10.1088/0004-6256/139/4/1338

Foreman-Mackey, D., Hogg, D. W., Lang, D., & Goodman,
    J. 2013, PASP, 125, 306, doi: 10.1086/670067

Fortney, J. J., Marley, M. S., & Barnes, J. W. 2007, ApJ,
    659, 1661, doi: 10.1086/512120

Fortney, J. J., & Nettelmann, N. 2010, SSRv, 152, 423,
    doi: 10.1007/s11214-009-9582-x

Fulton, B. J., Petigura, E. A., Blunt, S., & Sinukoff, E.
    2018, PASP, 130, 044504, doi: 10.1088/1538-3873/aaaaa8

Fulton, B. J., Petigura, E. A., Howard, A. W., et al. 2017,
    AJ, 154, 109, doi: 10.3847/1538-3881/aa80eb

Furlan, E., Ciardi, D. R., Everett, M. E., et al. 2017, AJ,
    153, 71, doi: 10.3847/1538-3881/153/2/71

Gagné, J., Mamajek, E. E., Malo, L., et al. 2018, ApJ, 856,
    23, doi: 10.3847/1538-4357/aaae09

Gaia Collaboration, Brown, A. G. A., Vallenari, A., et al.
    2018, A&A, 616, A1, doi: 10.1051/0004-6361/201833051

Ginzburg, S., Schlichting, H. E., & Sari, R. 2018, MNRAS,
    476, 759, doi: 10.1093/mnras/sty290

Girardi, L., Barbieri, M., Groenewegen, M. A. T., et al.
    2012, Astrophysics and Space Science Proceedings, 26,
    165, doi: 10.1007/978-3-642-18418-5_17

Goodman, J., & Weare, J. 2010, Communications in
    Applied Mathematics and Computational Science, Vol. 5,
    No. 1, p. 65-80, 2010, 5, 65,
    doi: 10.2140/camcos.2010.5.65

Grankin, K. N., Artemenko, S. A., & Melnikov, S. Y. 2007,
    Information Bulletin on Variable Stars, 5752

Gray, D. F. 2005, The Observation and Analysis of Stellar
    Photospheres (Cambridge University Press)

Gupta, A., & Schlichting, H. E. 2018, arXiv e-prints.
    https://arxiv.org/abs/1811.03202

Hartmann, L., Jones, B. F., Stauffer, J. R., & Kenyon, S. J.
    1991, AJ, 101, 1050, doi: 10.1086/115747

Howard, A. W., Johnson, J. A., Marcy, G. W., et al. 2010,
    ApJ, 721, 1467, doi: 10.1088/0004-637X/721/2/1467

Howell, S. B., Sobeck, C., Haas, M., et al. 2014, PASP, 126,
    398, doi: 10.1086/676406

Huang, C., Wu, Y., & Triaud, A. H. M. J. 2016, ApJ, 825,
    98, doi: 10.3847/0004-637X/825/2/98

Jeffries, R. D., Naylor, T., Mayne, N. J., Bell, C. P. M., &
    Littlefair, S. P. 2013, MNRAS, 434, 2438,
    doi: 10.1093/mnras/stt1180

Johns-Krull, C. M., McLane, J. N., Prato, L., et al. 2016,
    ApJ, 826, 206, doi: 10.3847/0004-637X/826/2/206

Jones, B. F., Shetrone, M., Fischer, D., & Soderblom, D. R.
    1996, AJ, 112, 186, doi: 10.1086/117999

Kipping, D. M. 2010, MNRAS, 407, 301,
    doi: 10.1111/j.1365-2966.2010.16894.x

Kley, W., & Nelson, R. P. 2012, ARA&A, 50, 211,
    doi: 10.1146/annurev-astro-081811-125523

Kolbl, R., Marcy, G. W., Isaacson, H., & Howard, A. W.
    2015, AJ, 149, 18, doi: 10.1088/0004-6256/149/1/18

Kraus, A. L., Herczeg, G. J., Rizzuto, A. C., et al. 2017,
    ApJ, 838, 150, doi: 10.3847/1538-4357/aa62a0

Kraus, A. L., Shkolnik, E. L., Allers, K. N., & Liu, M. C.
    2014, AJ, 147, 146, doi: 10.1088/0004-6256/147/6/146

Lallement, R., Vergely, J.-L., Valette, B., et al. 2014, A&A,
    561, A91, doi: 10.1051/0004-6361/201322032

Libralato, M., Nardiello, D., Bedin, L. R., et al. 2016,
    MNRAS, 463, 1780, doi: 10.1093/mnras/stw1932

Livingston, J. H., Dai, F., Hirano, T., et al. 2018, AJ, 155,
    115, doi: 10.3847/1538-3881/aaa841

—. 2019, MNRAS, 484, 8, doi: 10.1093/mnras/sty3464

Lomb, N. R. 1976, Ap&SS, 39, 447,
    doi: 10.1007/BF00648343

Lopez, E. D., & Fortney, J. J. 2013, ApJ, 776, 2,
    doi: 10.1088/0004-637X/776/1/2

Luger, R., Kruse, E., Foreman-Mackey, D., Agol, E., &
    Saunders, N. 2018, AJ, 156, 99,
    doi: 10.3847/1538-3881/aad230

Luhman, K. L. 2018, ArXiv e-prints.
    https://arxiv.org/abs/1811.01359

Malo, L., Doyon, R., Lafrenière, D., et al. 2013, ApJ, 762,
    88, doi: 10.1088/0004-637X/762/2/88

Mamajek, E. E., & Hillenbrand, L. A. 2008, ApJ, 687,
    1264, doi: 10.1086/591785

Mandel, K., & Agol, E. 2002, ApJL, 580, L171,
    doi: 10.1086/345520

Mann, A. W., Gaidos, E., Mace, G. N., et al. 2016a, ApJ,
    818, 46, doi: 10.3847/0004-637X/818/1/46

Mann, A. W., Newton, E. R., Rizzuto, A. C., et al. 2016b,
    AJ, 152, 61, doi: 10.3847/0004-6256/152/3/61

Mann, A. W., Gaidos, E., Vanderburg, A., et al. 2017, AJ,
    153, 64, doi: 10.1088/1361-6528/aa5276

Mann, A. W., Vanderburg, A., Rizzuto, A. C., et al. 2018,
    AJ, 155, 4, doi: 10.3847/1538-3881/aa9791

Mardling, R. A., & Aarseth, S. J. 2001, MNRAS, 321, 398,
    doi: 10.1046/j.1365-8711.2001.03974.x

Marley, M. S., Fortney, J. J., Hubickyj, O., Bodenheimer,
    P., & Lissauer, J. J. 2007, ApJ, 655, 541,
    doi: 10.1086/509759

Martin, D. C., Fanson, J., Schiminovich, D., et al. 2005,
    ApJL, 619, L1, doi: 10.1086/426387

Mentuch, E., Brandeker, A., van Kerkwijk, M. H.,
    Jayawardhana, R., & Hauschildt, P. H. 2008, ApJ, 689,
    1127, doi: 10.1086/592764

Mordasini, C. 2013, A&A, 558, A113,
    doi: 10.1051/0004-6361/201321617

Mordasini, C., Alibert, Y., Georgy, C., et al. 2012, A&A, 547, A112, doi: 10.1051/0004-6361/201118464

Mordasini, C., Marleau, G.-D., & Mollière, P. 2017, A&A, 608, A72, doi: 10.1051/0004-6361/201630077

Newville, M., Stensitzki, T., Allen, D. B., & Ingargiola, A. 2014, LMFIT: Non-Linear Least-Square Minimization and Curve-Fitting for Python, doi: 10.5281/zenodo.11813. https://doi.org/10.5281/zenodo.11813

Nguyen, D. C., Brandeker, A., van Kerkwijk, M. H., & Jayawardhana, R. 2012, ApJ, 745, 119, doi: 10.1088/0004-637X/745/2/119

Nidever, D. L., Marcy, G. W., Butler, R. P., Fischer, D. A., & Vogt, S. S. 2002, ApJS, 141, 503, doi: 10.1086/340570

Obermeier, C., Henning, T., Schlieder, J. E., et al. 2016, AJ, 152, 223, doi: 10.3847/1538-3881/152/6/223

Oh, S., Price-Whelan, A. M., Hogg, D. W., Morton, T. D., & Spergel, D. N. 2017, AJ, 153, 257, doi: 10.3847/1538-3881/aa6ffd

Olmedo, M., Lloyd, J., Mamajek, E. E., et al. 2015, ApJ, 813, 100, doi: 10.1088/0004-637X/813/2/100

Owen, J. E., & Wu, Y. 2013, ApJ, 775, 105, doi: 10.1088/0004-637X/775/2/105

Palla, F., & Stahler, S. W. 2002, ApJ, 581, 1194, doi: 10.1086/344293

Parviainen, H. 2015, MNRAS, 450, 3233, doi: 10.1093/mnras/stv894

Pecaut, M. J., & Mamajek, E. E. 2013, ApJS, 208, 9, doi: 10.1088/0067-0049/208/1/9

Pepper, J., Gillen, E., Parviainen, H., et al. 2017, AJ, 153, 177, doi: 10.3847/1538-3881/aa62ab

Petigura, E. A., Howard, A. W., & Marcy, G. W. 2013, Proceedings of the National Academy of Science, 110, 19273, doi: 10.1073/pnas.1319909110

Petigura, E. A., Sinukoff, E., Lopez, E. D., et al. 2017, AJ, 153, 142, doi: 10.3847/1538-3881/aa5ea5

Petigura, E. A., Crossfield, I. J. M., Isaacson, H., et al. 2018, AJ, 155, 21, doi: 10.3847/1538-3881/aa9b83

Petrovich, C., & Tremaine, S. 2016, ApJ, 829, 132, doi: 10.3847/0004-637X/829/2/132

Quinn, S. N., White, R. J., Latham, D. W., et al. 2012, ApJL, 756, L33, doi: 10.1088/2041-8205/756/2/L33

—. 2014, ApJ, 787, 27, doi: 10.1088/0004-637X/787/1/27

Randich, S., Pallavicini, R., Meola, G., Stauffer, J. R., & Balachandran, S. C. 2001, A&A, 372, 862, doi: 10.1051/0004-6361:20010339

Rebull, L. M., Stauffer, J. R., Cody, A. M., et al. 2018, AJ, 155, 196, doi: 10.3847/1538-3881/aab605

Rebull, L. M., Stauffer, J. R., Bouvier, J., et al. 2016, AJ, 152, 113, doi: 10.3847/0004-6256/152/5/113

Rizzuto, A. C., Mann, A. W., Vanderburg, A., Kraus, A. L., & Covey, K. R. 2017, AJ, 154, 224, doi: 10.3847/1538-3881/aa9070

Rizzuto, A. C., Vanderburg, A., Mann, A. W., et al. 2018, AJ, 156, 195, doi: 10.3847/1538-3881/aadf37

Santerne, A., Moutou, C., Tsantaki, M., et al. 2016, A&A, 587, A64, doi: 10.1051/0004-6361/201527329

Scargle, J. D. 1982, ApJ, 263, 835, doi: 10.1086/160554

Schlichting, H. E., Sari, R., & Yalinewich, A. 2015, Icarus, 247, 81, doi: 10.1016/j.icarus.2014.09.053

Skrutskie, M. F., Cutri, R. M., Stiening, R., et al. 2006, AJ, 131, 1163, doi: 10.1086/498708

Slesnick, C. L., Carpenter, J. M., Hillenbrand, L. A., & Mamajek, E. E. 2006, AJ, 132, 2665, doi: 10.1086/508937

Soderblom, D. R., Jones, B. F., Balachandran, S., et al. 1993, AJ, 106, 1059, doi: 10.1086/116704

Spiegel, D. S., & Burrows, A. 2012, ApJ, 745, 174, doi: 10.1088/0004-637X/745/2/174

Thompson, S. E., Coughlin, J. L., Hoffman, K., et al. 2018, ApJS, 235, 38, doi: 10.3847/1538-4365/aab4f9

Tokovinin, A. 2018, ApJS, 235, 6, doi: 10.3847/1538-4365/aaa1a5

Udry, S., Mayor, M., & Santos, N. C. 2003, A&A, 407, 369, doi: 10.1051/0004-6361:20030843

van Eyken, J. C., Ciardi, D. R., von Braun, K., et al. 2012, ApJ, 755, 42, doi: 10.1088/0004-637X/755/1/42

Vanderburg, A., Bieryla, A., Duev, D. A., et al. 2016, ApJL, 829, L9, doi: 10.3847/2041-8205/829/1/L9

Vanderburg, A., Mann, A. W., Rizzuto, A., et al. 2018, AJ, 156, 46, doi: 10.3847/1538-3881/aac894

Vogt, S. S., Allen, S. L., Bigelow, B. C., et al. 1994, in Proc. SPIE, Vol. 2198, Instrumentation in Astronomy VIII, ed. D. L. Crawford & E. R. Craine, 362–375

Wahhaj, Z., Cieza, L., Koerner, D. W., et al. 2010, ApJ, 724, 835, doi: 10.1088/0004-637X/724/2/835

Waite, I. A., Marsden, S. C., Carter, B. D., et al. 2011, MNRAS, 413, 1949, doi: 10.1111/j.1365-2966.2011.18366.x

Weiss, L. M., Marcy, G. W., Petigura, E. A., et al. 2018, AJ, 155, 48, doi: 10.3847/1538-3881/aa9ff6

Wichmann, R., Krautter, J., Schmitt, J. H. M. M., et al. 1996, A&A, 312, 439

Wichmann, R., Torres, G., Melo, C. H. F., et al. 2000, A&A, 359, 181

Wright, N. J., Drake, J. J., Mamajek, E. E., & Henry, G. W. 2011, ApJ, 743, 48, doi: 10.1088/0004-637X/743/1/48

Yee, J. C., & Jensen, E. L. N. 2010, ApJ, 711, 303, doi: 10.1088/0004-637X/711/1/303

Yu, L., Winn, J. N., Gillon, M., et al. 2015, ApJ, 812, 48, doi: 10.1088/0004-637X/812/1/48

Yu, L., Donati, J.-F., Hébrard, E. M., et al. 2017, MNRAS, 467, 1342, doi: 10.1093/mnras/stx009

Yuan, H. B., Liu, X. W., & Xiang, M. S. 2013, MNRAS, 430, 2188, doi: 10.1093/mnras/stt039

Zhang, Z., Liu, M. C., Best, W. M. J., et al. 2018, ApJ, 858, 41, doi: 10.3847/1538-4357/aab269

Ziegler, C., Law, N. M., Baranec, C., et al. 2018, AJ, 156, 259, doi: 10.3847/1538-3881/aad80a